SUPPRESSION OF SINGULARITY IN STOCHASTIC FRACTIONAL BURGERS EQUATIONS WITH MULTIPLICATIVE NOISE

SUPPRESSION OF SINGULARITY IN STOCHASTIC FRACTIONAL BURGERS EQUATIONS WITH MULTIPLICATIVE NOISE

By SADIA MASUD, M.Sc

A Thesis Submitted to the School of Graduate Studies in Partial Fulfillment of the Requirements for the Degree Master of Science

Mathematics

MASTER OF SCIENCE (2024)

Hamilton, Ontario, Canada (McMaster University)

TITLE:	SUPPRESSION OF SINGULARITY IN STOCHASTIC FRACTIONAL BURGERS EQUATIONS WITH MULTIPLICATIVE NOISE
AUTHOR:	Sadia Masud M.Sc (Mathematics), University of Dhaka, Dhaka, Bangladesh
SUPERVISOR:	Professor Bartosz Protas
NUMBER OF PAGES:	xi, 70

Abstract

Inspired by studies on the regularity of solutions to the fractional Navier-Stokes system and the impact of noise on singularity formation in hydrodynamic models, we investigated these issues within the framework of the fractional 1D Burgers equation. Initially, our research concentrated on the deterministic scenario, where we conducted precise numerical computations to understand the dynamics in both subcritical and supercritical regimes. We utilized a pseudo-spectral approach with automated resolution refinement for discretization in space combined with a hybrid Crank-Nicolson/ Runge-Kutta method for time discretization.We estimated the blow-up time by analyzing the evolution of enstrophy (H^1 seminorm) and the width of the analyticity strip. Our findings in the deterministic case highlighted the interplay between dissipative and nonlinear components, leading to distinct dynamics and the formation of shocks and finite-time singularities.

In the second part of our study, we explored the fractional Burgers equation under the influence of linear multiplicative noise. To tackle this problem, we employed the Milstein Monte Carlo approach to approximate stochastic effects. Our statistical analysis of stochastic solutions for various noise magnitudes showed that as noise amplitude increases, the distribution of blow-up times becomes more non-Gaussian. Specifically, higher noise levels result in extended mean blow-up time and increase its

variability, indicating a regularizing effect of multiplicative noise on the solution. This highlights the crucial role of stochastic perturbations in influencing the behavior of singularities in such systems. Although the trends are rather weak, they nevertheless are consistent with the predictions of the theorem of [41]. However, there is no evidence for a complete elimination of blow-up, which is probably due to the fact that the noise amplitudes considered were not sufficiently large. This highlights the crucial role of stochastic perturbations in influencing the behavior of singularities in such systems.

Acknowledgements

I would like to express my heartfelt gratitude to my supervisor, Dr. Bartosz Protas, for his invaluable advice, insightful comments, and guidance throughout the development of this thesis. I am also deeply appreciative of Dr. Blaise Bourdin and Dr. Anastasis Kratsios for their constructive feedback and remarks on my work. Additionally, I extend my thanks to McMaster University for providing me with the opportunity for both academic and cultural exchange. Finally, I am profoundly grateful to my loved ones and friends for their unwavering support throughout this entire journey.

Table of Contents

List of Figures

Chapter 1

Introduction

The Navier-Stokes equations form the cornerstone of the mathematical modeling of viscous, incompressible fluid flow, playing a pivotal role in a multitude of scientific and engineering applications. These equations, which describe the evolution of velocity and pressure fields in incompressible fluids, reflect the principles of mass and momentum conservation. Despite their extensive utility, a full mathematical understanding of these equations, especially in the three-dimensional (3D) context, is still an area of active research. Global classical solutions are established for the Navier-Stokes equations in two dimensions [5, 45, 15], ensuring well-defined behavior for arbitrarily long times, but this certainty does not extend to 3D [34, 31]. In 3D, classical solutions have been constructed in finite time only [35], with their long-term dynamics remaining a significant unresolved issue. Although there are known global weak solutions in 3D [10], they need not be smooth nor unique, which leaves the possibility of formation of singularities in finite time open [14, 39]. A definitive resolution of the question whether all initial conditions yield global, smooth solutions of the 3D Navier-Stokes system remains one of the seven Millennium Prize Problems [16],

representing a critical, yet unsolved, question in mathematics, carrying a substantial reward for a conclusive answer.

Due to the complexities involved in studying the 3D Navier-Stokes system, we aim to investigate the effect of multiplicative noise on the singularity formation in solutions of the fractional Burgers equation. In mathematical terms, a *singularity* in this context refers to a point in time and space where the solution to the differential equation becomes undefined or such that it cannot satisfy the equation locally. This typically occurs when the derivatives of the solution increase without bound as they approach a certain point, leading to a breakdown in the classical description of the system's evolution. Understanding singularity formation is crucial for understanding the limits of predictability and stability within these dynamic systems, particularly under the influence of stochastic disturbances. This research is underpinned by the significance of the Navier-Stokes equations in modeling fluid flow, where challenges in fully grasping their 3D dynamics motivate the study of simpler models such as the fractional Burgers equation. This model provides a manageable framework for investigating the impact of stochastic forcing impact on fluid dynamics, aiming to deepen our mathematical and physical insights into singularity formation. The behavior of this model hinges on the fractional dissipation exponent, α, which controls how dissipation, which has a regularizing effect, acts on different length scales. When $\alpha \geq \frac{1}{2}$ —— in the critical and subcritical regimes —— the system maintains global well-posedness. In contrast, in the supercritical regime where $\alpha < \frac{1}{2}$, the system exhibits a finite-time blow-up [27]. This situation mirrors some aspects of the 3D Navier-Stokes system, which also remains globally well-posed with fractional dissipation for $\alpha \geq \frac{5}{4}$ [26]. As expected for $\alpha = 1$, the fractional Burgers equation becomes

the well-known viscous Burgers equation, a widely studied model for one-dimensional fluid flow [4]. Further, the fractional Burgers equation has been a subject of interest in turbulence-related studies [8]. To date, significant attention has been given to the complex interaction between stochastic forcing and the behavior of hydrodynamic models, particularly in relation to singularity formation. A crucial aspect of this research focuses on the potential of a stochastic input to excite the systems, through its interaction with the nonlinearity and dissipation, possibly accelerating, delaying, or completely averting singularities [7, 17, 13, 1, 2]. Key contributions in this domain have been the restoration of global well-posedness in systems that otherwise exhibit finite-time blow-up in the deterministic framework, using stochastic excitation [40, 17, 13, 28]. This is notably evident in the case of the stochastically forced Burgers equation, which has been instrumental in advancing the understanding of 3D turbulence, particularly in its connection to the Kardar–Parisi–Zhang equation [22]. The extreme behavior of the solution is measured through the growth of various Sobolev norms of the solutions and their connection to the deterministic regime, as explored in references [3] and [36]. Additionally, issues surrounding the formation of singularities in the dispersive Burgers equation were examined through numerical studies, as detailed in reference [28]. Research in this area also encompasses the dynamics of statistical equilibria in turbulent flows, focusing on how stochastic forcing influences the scaling of energy spectra, intermittency of structure functions, and the extreme behavior of these systems [11, 12, 50, 19]. These investigations have not only deepened the understanding of fluid dynamics under stochastic conditions but also opened new pathways in the study of intricate hydrodynamic systems.

Investigating the effects of noise on general stochastic partial differential equations (SPDEs) necessitates a clear differentiation between additive and multiplicative noise types. The effect of additive noise has been thoroughly explored, with significant progress made in the analysis of weak convergence and the identification of random attractors in SPDEs subjected to this type of noise [47, 18, 48]. Additionally, advancements have been made in developing numerical approximation methods for SPDEs driven by additive noise, achieving higher orders of convergence compared to traditional approaches [49, 24]. On the other hand, our understanding of SPDEs affected by multiplicative noise is still evolving. Multiplicative noise refers to random perturbations in a system where the intensity of the noise depends on the state of the system itself, often leading to more complex and varied behavior compared to additive noise. Research indicates that in SPDEs, the presence of linear multiplicative noise plays a crucial role in preventing the formation of finite-time singularities within the supercritical regime [41]. Studies in this field have mainly focused on overcoming the challenges associated with numerically approximating SPDEs under the influence of multiplicative noise, highlighting the urgent need for further exploration in this area [43, 25].

Building on the foundational understanding of noise effects in general SPDEs, researchers have extended their investigations into more specific domains, such as the study of additive and multiplicative noise within the context of the fractional Burgers equation. The insights from general SPDEs with additive noise have informed numerical schemes [38] and theoretical analyses [40, 21] aiming to capture the behavior of solutions under stochastic activation, improving our understanding of dissipation and diffusion mechanisms in the presence of randomness. Conversely, consideration

of multiplicative noise has been a focal point for advancing our comprehension of how intrinsic variability within the system or its environment can lead to fundamentally different outcomes compared to those driven by additive noise. The existence and uniqueness of a mild global solution to the Cauchy problem for the stochastic fractional Burgers equation on an interval, subjected to multiplicative space-time white noise and periodic boundary conditions, were thoroughly investigated by Brzeźniak and Debbi [9]. In reference [41], the authors examined how properties of solutions to the fractional Burgers equation vary depending on the noise type. Specifically, they demonstrated that when multiplicative noise of a certain structure is present, it prevents the formation of finite-time singularities in the supercritical regime. However, the regularizing effect of multiplicative noise has been numerically validated in other equations [13], suggesting a broader potential for its application in mitigating singular behavior in complex systems. This potential for multiplicative noise to regularize singularities, especially when its effect is less straightforward compared to additive noise, underscores the importance of further study in this area.

In the numerical exploration of SDEs that characterize the intricate dynamics of singularity formation in fractional Burgers equations with multiplicative noise, selecting an appropriate numerical scheme is crucial. The literature reveals a spectrum of numerical methods tailored to these equations, from the foundational Euler-Maruyama scheme to the more sophisticated Milstein and pseudo-spectral methods. While the Euler-Maruyama method is known for its simplicity and broad applicability, as evidenced in the seminal works [29, 23], it often falls short in accurately capturing the detailed behaviors of nonlinear systems influenced by multiplicative noise [29, 30]. On the other hand, the Milstein method, recognized for its enhanced convergence and

accuracy in dealing with SDEs featuring multiplicative noise [33, 20, 25, 46], is particularly promising for the objectives of the present study. Coupled with pseudo-spectral methods, which efficiently manage spatial discretization, the Milstein method is adept at accurately simulating the stochastic dynamics that underpin singularity formation.

This study primarily aims to computationally verify the regularization effect of linear multiplicative noise on singularity formation in the stochastic fractional Burger equation, as studied in reference [41]. Employing the Milstein pseudo-spectral method as our principal numerical approach not only leverages its enhanced accuracy and convergence but also optimizes the handling of discretization with respect to noise, thus allowing for precise simulation of the complex dynamics at play. This strategic choice of methodology is central to addressing the key question of our research: the impact of multiplicative noise in modulating the behavior of singularities within such stochastic systems. To fulfill our research objectives, Chapter 2 delineates our primary problems—the deterministic and stochastic fractional Burgers equations. Here, we recall some established results and introduce two critical quantities essential for analyzing singularity formation. In Chapter 3, we detail the numerical methods applied to solve these equations, validate the numerical scheme for the stochastic system and outline our approach for calculating estimates of blow-up times. Chapter 4 is dedicated to presenting the results derived from our numerical analyses. Finally, in Chapter 5, we summarize the key findings and discuss directions for future research.

Our findings reveal some insights into both deterministic and stochastic cases of the fractional Burgers equation. In the deterministic case, we observed distinct dynamics in both physical and Fourier spaces. The results highlighted the interplay between dissipative and nonlinear elements, where the dominance of the nonlinear

term led to the intensification of solution fronts, and the dissipative term contributed to the eventual flattening of these fronts. This duality is particularly evident when comparing the subcritical regime with the supercritical regime, with the formation of finite-time singularities in the form of shocks evident in the latter.

In the stochastic analysis, the introduction of multiplicative noise altered the system's behavior. Increased noise amplitude $\rho \in \mathbb{R}$ demonstrated some regularizing effect on the solution, which delayed the blow-up and increased its variability. Specifically, as ρ increased, the mean blow-up time was extended, and its distribution became increasingly skewed and non-Gaussian. This indicates that noise introduces a stabilizing influence, delaying the onset of singularities that are otherwise observed in the deterministic case. These findings underscore the critical role of noise in modulating the dynamics of the system, providing a detailed understanding of how stochastic perturbations can influence the evolution of solutions.

These insights provide an improved understanding of the system's behavior under different conditions, establishing a crucial link between deterministic and stochastic frameworks. By comparing the deterministic and stochastic cases, we gain a deeper appreciation of how noise can regularize and modify the evolution of solutions, leading to new perspectives on the control and prediction of singularity formation in nonlinear partial differential equations.

Chapter 2

Fractional Burgers Equation

In this chapter, we introduce the deterministic version of the fractional Burgers equation as a basis for comparing it with its stochastic counterpart, which incorporates multiplicative noise. This comparative analysis aims to provide a comprehensive understanding of both systems. Furthermore, we will delve into two critical measures — the width of analyticity strip and enstrophy, to investigate the regularity of the solution.

Before proceeding further, it is necessary to define the functional spaces that are instrumental in our analysis. Before proceeding further, it is necessary to define the functional spaces that are instrumental in our analysis.

Definition 2.0.1. *L^p space: This space is defined over a measure space $(\Omega, \mathcal{F}, \mu)$. For $1 \leq p < \infty$, it consists of equivalence classes of all measurable functions $f : \Omega \to \mathbb{R}$ (or $\mathbb{C}$) such that the integral of the p-th power of their absolute values is finite. This*

is expressed as:

$$L^p(\Omega) := \left\{ f : \Omega \to \mathbb{R} \text{ measurable} \mid \int_\Omega |f(x)|^p \, d\mu(x) < \infty \right\} \tag{2.0.1}$$

Here, Ω is the domain over which functions are defined and can be any set equipped with a measure μ, where functions $f : \Omega \to \mathbb{R}$ or $\mathbb{C}$ are identified as measurable. $\mathcal{F}$ is the σ-algebra of measurable subsets of Ω, a structured collection that includes Ω itself and the empty set, and is closed under complementation and countable unions. In equation (2.0.1), μ is a measure defined on the σ-algebra $\mathcal{F}$, assigning a non-negative extended real number to subsets in $\mathcal{F}$ according to the axioms of non-negativity, null empty set, and countable additivity.

The norm in the space L^p is defined as,

$$\|f\|_p = \left(\int_\Omega |f(x)|^p \, d\mu(x) \right)^{\frac{1}{p}} \tag{2.0.2}$$

Definition 2.0.2. *L^2 space: The space $L^2(\Omega, \mathcal{F}, \mu)$ is of special case of L^p space when $p = 2$,*

$$L^2(\Omega) := \left\{ f : \Omega \to \mathbb{R} \text{ (or } \mathbb{C}\text{) measurable} \mid \int_\Omega |f(x)|^2 \, d\mu(x) < \infty \right\} \tag{2.0.3}$$

This space is a Hilbert space, which means it is equipped with an inner product defined as follows:

$$\langle f, g \rangle := \int_\Omega f(x) \overline{g(x)} \, d\mu(x) \tag{2.0.4}$$

where $\overline{g(x)}$ denotes the complex conjugate of $g(x)$. The norm induced by this inner

product is given by:

$$\|f\|_2 = \left(\int_\Omega |f(x)|^2 \, d\mu(x) \right)^{\frac{1}{2}}. \tag{2.0.5}$$

This is a special case of (2.0.2) which measures the "energy" of the function across the domain Ω.

Definition 2.0.3. *Fourier coefficients: For a function* v *defined on the interval* $[0, 2\pi]$*, the Fourier coefficients* $\widehat{v}_k$ *are given by*

$$\widehat{v}_k = \frac{1}{2\pi} \int_0^{2\pi} v(x) e^{-ikx} \, dx, \quad k \in \mathbb{Z}$$

where dx *is the Lebesgue measure restricted to* $[0, 2\pi]$*, and the function* v *can be expressed as a Fourier series in terms of its Fourier coefficients:*

$$v(x) = \sum_{k=-\infty}^{\infty} \widehat{v}_k e^{ikx}, \quad x \in [0, 2\pi].$$

Definition 2.0.4. H^s *space: The Sobolev space* $H^s(0, 2\pi)$ *with* $s \in [0, \infty)$ *is defined as*

$$H^s(0, 2\pi) := \left\{ v \in L^2([0, 2\pi]) : \|v\|_{H^s(0,2\pi)} = \left(\sum_{k=-\infty}^{\infty} (1 + |k|^2)^s |\widehat{v}_k|^2 \right)^{\frac{1}{2}} < \infty \right\} \tag{2.0.6}$$

In this expression, s *represents the degree of smoothness (differentiability).*

Note that this definition is equivalent to standard definitions by basic properties of the Laplacian.

2.1 Deterministic Case of Fractional Burgers Equation

Given a sufficiently smooth function $v : [0, 2\pi] \to \mathbb{R}$, the Fourier transform of the fractional Laplacian $(-\Delta)^\alpha$ applied to v is represented as follows:

$$\widehat{(-\Delta)^\alpha v}_k = |k|^{2\alpha} \widehat{v}_k, \tag{2.1.1}$$

where $\widehat{[\cdot]}_k$ refers to Fourier coefficients with wavenumber $k \in \mathbb{Z}$. Here $\alpha \in (0, \infty]$

The 1D fractional Burgers equation has the form:

$$\frac{\partial u}{\partial t} + \frac{1}{2}\frac{\partial}{\partial x}u^2 + \nu(-\Delta)^\alpha u = 0 \quad \text{for } (t, x) \in (0, T] \times [0, 2\pi] \tag{2.1a}$$

and is considered subject to periodic boundary conditions:

$$u(t, 0) = u(t, 2\pi) \quad \text{for } t \in (0, T], \tag{2.1b}$$

and an initial condition:

$$u(0, x) = g(x) \quad \text{for } x \in [0, 2\pi]. \tag{2.1c}$$

We focus on periodic solutions for several reasons. Periodic boundary conditions simplify the analysis and numerical simulations by avoiding edge effects that can complicate the solution behavior near boundaries. Moreover, periodic solutions are often used in modeling physical phenomena with inherent periodicity or in cases where the domain can be conceptually extended to infinity by repeating the pattern. This

approach ensures that the solution remains consistent and well-defined over the entire spatial domain $[0, 2\pi]$. In this equation, u represents the dependent variable, t denotes time, and x represents the spatial variable. The parameter ν represents the viscosity, and α represents the order of the fractional Laplacian $(-\Delta)^\alpha$ where $\Delta = \frac{\partial^2}{\partial x^2}$. The function $g \in H^1(0, 2\pi)$ is the initial condition of u at $t = 0$, where $H^1(0, 2\pi)$ is the Sobolev space of square-integrable periodic functions on $(0, 2\pi)$ such that their first weak derivatives are also square-integrable. The periodic boundary conditions in Equation (2.1b) indicate that values of the solution u at the boundaries $x = 0$ and $x = 2\pi$ are equal for all time t in the interval $(0, T]$. The solution $u(t, x)$ preserves the mean value of the initial condition over the spatial domain. This conservation is derived below:

$$\frac{\partial}{\partial t}\int_0^{2\pi} u(t,x)\,dx = -\frac{1}{2}\int_0^{2\pi} \frac{\partial}{\partial x}u(t,x)^2\,dx - \int_0^{2\pi} \nu(-\Delta)^\alpha u(t,x)\,dx. \tag{2.1.2}$$

For the first term, using integration by parts:

$$-\frac{1}{2}\int_0^{2\pi} \frac{\partial}{\partial x}u(t,x)^2\,dx = -\frac{1}{2}\left[u(t,2\pi)^2 - u(t,0)^2\right] = 0, \tag{2.1.3}$$

due to periodicity of $u(t, x)$. For second term, we consider:

$$\begin{aligned} -\int_0^{2\pi} \nu(-\Delta)^\alpha u(t,x)\,dx &= -\int_0^{2\pi} \nu\left(-\frac{\partial^2}{\partial x^2}\right)^\alpha u(t,x)\,dx \\ &= \int_0^{2\pi} \nu\frac{\partial}{\partial x}\left(\frac{\partial}{\partial x}\right)^{\alpha-1} u(t,x)\,dx = 0. \end{aligned} \tag{2.1.4}$$

Combining both terms, we get:

$$\frac{d}{dt}\int_0^{2\pi} u(t,x)\,dx = 0. \tag{2.1.5}$$

This integral result is pivotal because it establishes that the initial average state of the system is zero. Also, it ensures that any changes in the system's state over time are purely redistributive in nature, and maintaining the initial condition's symmetry throughout the temporal evolution of the model. Additionally, $T > 0$ represents the length of the time window.

The key results, addressing questions about the existence of solutions for system (2.1) are established in [27, Theorem 1] and briefly summarized below.

Theorem 2.1.1. *(Subcritical Case)*

Assume that $\alpha > \frac{1}{2}$ and the initial data $g \in H^s(0,2\pi)$, where $s > \frac{3}{2} - 2\alpha$ and $s \geq 0$. Then, there exists a unique global solution u of problem (2.1) that belongs to $C((0,\infty); H^s(0,2\pi))$ and is real analytic in x for $t > 0$.

Theorem 2.1.2. *(Critical Case)*

Assume that $\alpha = \frac{1}{2}$ and $g \in H^s(0,2\pi)$, where $s > \frac{1}{2}$. Then, there exists a global solution u of system (2.1) that belongs to $C((0,\infty); H^s(0,2\pi)) \cap C((0,\infty); C(0,\infty))$ and is real analytic in x for any $t > 0$.

Theorem 2.1.3. *(Supercritical Case)*

Assume that $0 < \alpha < \frac{1}{2}$. Then, there exists a smooth periodic initial data $g \in H^s(0,2\pi)$ such that the solution u of (2.1) blows up in $H^s(0,2\pi)$ for each $s > \frac{3}{2} - 2\alpha$ in a finite time.

In the supercritical regime, solutions of system (2.1) are analytic until the blow-up time. Assuming $g \in H^1(0, 2\pi)$, Theorem 2.1.3 asserts that solutions blow up for some initial data when $\frac{1}{4} < \alpha < \frac{1}{2}$.

However, for $\alpha \in [0, \frac{1}{4}]$, the situation is more complex for several reasons. Firstly, if $0 < \alpha \leq \frac{1}{4}$ and $g \in H^1(0, 2\pi)$, Theorem 2.1.3 does not provide conclusive results. Secondly, numerical findings indicate that solutions of system (2.1) may still exhibit blow-up for values of α in $(0, \frac{1}{4})$ with a specific initial condition $g \in H^1(0, 2\pi)$ [38].

Lastly, a conjecture proposed in [49] suggests that if $0 \leq \alpha \leq \frac{1}{4}$, system (2.1) might not be locally well-posed in $H^1(0, 2\pi)$ for certain initial data. This implies that the condition for parameter values $s > \frac{3}{2} - 2\alpha$ in Theorem 2.1.3 might not be space , as blow-up could potentially occur outside that condition under specific initial data, for example, when $s = 1$, $0 < \alpha \leq \frac{1}{4}$, and $g(x) = \sin(x)$.

2.2 Stochastic Fractional Burgers Equation with Multiplicative Noise

We consider the following stochastic version of the fractional Burgers system (2.1):

$$\frac{\partial u}{\partial t} + \frac{1}{2}\frac{\partial}{\partial x}u^2 + \nu(-\Delta)^{\alpha}u = G(u)\frac{dW(t,x)}{dt} \quad \text{for } (t,x) \in (0,T] \times [0,2\pi], \tag{2.4a}$$

subject to periodic boundary conditions:

$$u(t,0) = u(t,2\pi) \quad \text{for } t \in (0,T], \tag{2.4b}$$

and an initial condition:

$$u(0,x) = g(x) \quad \text{for } x \in [0, 2\pi]. \tag{2.4c}$$

Note that at any point $(t,x) \in (0,T] \times [0,2\pi]$, our solution is a random variable $u = u(t,x;\omega)$, where $\omega \in \Omega$, for some probability space, Ω. It is important to mention that in this context, α is in the interval $(1/4, 1/2)$ for the supercritical case and $[1/2, 1)$ for the subcritical case. Here the right hand side of (2.4a) is the noise term which can be additive or multiplicative in nature. Here, G is a measurable mapping from H to $L^2(K,H)$ (i.e., all Hilbert–Schmidt operators from K to H), where K and H are separable Hilbert space. In this analysis, we define the noise function $G(u)$ in the context of multiplicative noise as $G(u) = \rho u$, where $\rho \in \mathbb{R}$ represents the magnitude of the noise. Conversely, for the additive noise scenario, the noise function is defined simply as $G(u) = \rho$, representing a constant noise term independent of u [38]. Let us define the Wiener process as:

$$W(t,x) = \sum_{k=1}^{N} \gamma_k \beta_k(t) \chi_k(x), \tag{2.5}$$

where $\{\beta_k(t)\}_{k=1}^{N}$ are independent and identically distributed (i.i.d.) standard Brownian motions on the filtered probability space $(\Omega, \mathcal{F}, \mathcal{F}_t \in [0,T], P)$ [32], in which $\mathcal{F}$ is the sigma-field representing the total information (set of all events) at the end of the observation period, and $\mathcal{F}_t$ represents the information available up to time t, evolving as time progresses within the filtration $(\mathcal{F}_t)_{t\in[0,T]}$, $\{\chi_k\}_{k\in\mathbb{N}}$ are elements of a trigonometric orthonormal basis of $L^2([0,2\pi])$, and $\{\gamma_k\}_{k\in\mathbb{N}}$ are scaling coefficients. We define the basis functions as follows: set $\chi_0(x) = 1$, for even indices

$\chi_{2k}(x) = \sqrt{2}\cos(kx)$, and for odd indices $\chi_{2k-1}(x) = \sqrt{2}\sin(kx)$, where $x \in [0, 2\pi]$ and k ranges over positive integers. For the purpose of analysis, we employ a finite number N of these Fourier modes in ansatz (2.5), which corresponds to the number of Fourier components used for spatial discretization of system (2.4). This alignment ensures that the noise influences each Fourier component. Additionally, the scaling coefficients are selected to ensure ℓ^2-summability

$$\begin{aligned} \gamma_0 &= 0, \\ \gamma_{2k-1} = \gamma_{2k} &= \frac{1}{k^\theta}, \quad k > 0, \quad \theta > \frac{1}{2}, \end{aligned} \tag{2.6}$$

so that $W(t, x)$ has finite variance in the limit $N \to \infty$. This definition of the Wiener process $W(t)$ — ensures that the noise is a square-integrable function in the L^2 space for all times. Specifically, this choice of $W(t)$ allows us to assert that the enstrophy is a well defined quantity particularly when $\alpha > \frac{1}{2}$. Moreover, with $W(t)$ satisfying these conditions, the mild solution of the system (2.4), as described in equation (2.8), is well-defined in the H^1 space. This setting is particularly important as it affects the solution's regularity. To define solutions of the stochastic problem more precisely, it is necessary to rewrite system (2.4) in the corresponding differential form:

$$du = \left(-\frac{1}{2}\frac{\partial x}{\partial u^2} - \nu(-\Delta)^\alpha u \right) dt + G(u)dW \quad \text{for } (t, x) \in (0, T] \times [0, 2\pi], \tag{2.7a}$$

subject to periodic boundary conditions:

$$u(t, 0) = u(t, 2\pi) \quad \text{for } t \in (0, T], \tag{2.7b}$$

and an initial condition:

$$u(0,x) = g(x) \quad \text{for } x \in [0, 2\pi]. \tag{2.7c}$$

Definition 2.2.1. *[41] Fix a stochastic basis $(\Omega, \mathcal{F}, P, (\mathcal{F}_t), W)$:*

(i) Let τ be an $(\mathcal{F}_t)$-stopping time, and $u = (u(t))_{t\geq 0}$ is a predictable H^{s_0}-valued process, see section A.2.1. Here τ is a random variable that takes values in the non-negative real numbers $[0, \infty)$. It has the property that for each time t, the event $\{\tau \leq t\}$ belongs to the sigma-algebra $\mathcal{F}_t$. This defines τ as the $\mathcal{F}$- predictable random time at which certain conditions of a stochastic process may cease to hold, rendering the solution to a differential equation potentially undefined or invalid beyond this time. And let u be a predictable process that takes values in the Sobolev space H^{s_0}, $s_0 \geq 1$. A process is termed predictable if the value of u at any time t can be determined using the information available up to just before t i.e., it is measurable with respect to the sigma-algebra $(\{\mathcal{F}_s\}_{0\leq s<t})$. Hence (u, τ) is the local strong solution of (2.2), such that:

- $u(\cdot \wedge \tau) \in L^2(\Omega; L^2_{loc}([0,\infty); H_2^{s_0+\alpha}))$
- $u(\cdot \wedge \tau) \in C([0,\infty); H_2^{s_0})$ *P-a.s. (Here, P-a.s. stands for "almost surely" with respect to the probability measure P, meaning this property holds with probability 1 i.e., except on a set of measure zero.)*
- *For every $t \geq 0$, $\phi \in \bigcap_{l=1}^{\infty} H_2^l$:*

$$\Big\langle u(t\wedge\tau), \phi \Big\rangle + \int_0^{t\wedge\tau} \Big\langle u\frac{\partial u}{\partial x} - (-\Delta)^{\alpha} u, \phi \Big\rangle dt = \Big\langle u_0, \phi \Big\rangle + \int_0^{t\wedge\tau} G(u) dW \cdot \phi dt \quad P\text{-a.s.}$$

The space $L^2_{loc}([0,\infty); H_2^{s_0+\alpha})$ denotes the set of functions that are locally (in time) square-integrable in $H_2^{s_0+\alpha}$.

(ii) We say that local pathwise uniqueness holds if, given any pair (u^1, τ^1), (u^2, τ^2) of local strong solutions of equation (2.2) the specified equation with the same initial condition, the following statement holds truecondition is satisfied:

$$P[u^1(t) = u^2(t) \text{ for all } t \in [0, \tau^1 \wedge \tau^2]] = 1.$$

(iii) A maximal strong solution of (2.2) is a pair $({u^R}_{R\in\mathbb{N}}, (\tau_R)_{R\in\mathbb{N}})$ such that for each $R \in \mathbb{N}$:

- *(u^R, τ_R) is a local strong solution*
- *τ_R is increasing such that $T^\infty := \lim_{R\to\infty} \tau_R > 0$ P-a.s.*
- *$\sup_{t\in[0,\tau_R]} |(A^{\frac{s_0}{2}} u^R(t)| \geq R$ P-a.s. on the set $[T^\infty < \infty]$.*

where $A := \nu(-\Delta)^\alpha$ is associated with periodic boundary conditions. Then, the relevant concept of a solution is the mild solution defined as:

$$u(t) = e^{-tA}g - \frac{1}{2}\int_0^t e^{-(t-s)A}\frac{\partial}{\partial x}u^2 ds + \int_0^t G(u)e^{-(t-s)A}dW(s), \tag{2.8}$$

where the semigroup e^{-tA} is defined in terms of its action on the elements of the basis $\{\phi_k\}_{k\in\mathbb{Z}} = \{e^{ikx}\}_{k\in\mathbb{Z}}$ of $L^2([0, 2\pi])$ as $e^{-tA}e^{ikx} = e^{-\nu t|k|^{2\alpha}}e^{ikx}$, while the second integral is understood in Itô's sense ,cf. Appendix A.

The existence of such solutions is then asserted by the following theorem, adapted from [41, Theorem 5.5]. It is assumed that the operator G satisfies two key conditions for $0 < \alpha < 1$ and $s_0 \geq 1$:

(G.1) For all $s \in [s_0, s_0+1]$, G is an operator from H^s to $L^2(K, H^s)$, and there exists a locally bounded function σ_1 on $\mathbb{R}$ such that for all $v \in H^s$, $\|A^{\frac{s}{2}}G(v)\|_{L^2(K,H)} \leq \sigma_1(|A^{\frac{s_0}{2}}v|)(|A^{\frac{s}{2}}v|+1)$.

(G.2) There exists locally bounded functions σ_2, σ_3 on $\mathbb{R}$ such that for $v_1, v_2 \in H^{s_0}$, $\|G(v_1)-G(v_2)\|_{L^2(K,H)} \leq (\sigma_2(|A^{\frac{s_0}{2}}v_1|)+\sigma_3(|A^{\frac{s_0}{2}}v_2|))|v_1-v_2|$.

Theorem 2.2.2 ([41]). *Fix $0<\alpha<1$. Assume that $G(u)$ satisfies $(G.1)$ and $(G.2)$ with $s_0 \geq \left(\frac{3}{2}-\alpha\right) \vee 1$. Assume that u_0 is an $H_2^{s_0}$-valued, $\mathcal{F}_0$-measurable random variable with $E|A^{\frac{s_0}{2}}u_0|^2 < \infty$, where E denotes the expectation of the random variable which, in this case, is the squared norm of $A^{\frac{s_0}{2}}u_0$.*

(i) Then local pathwise uniqueness holds, and there exists a maximal strong solution $(u, (\tau_R)_{R\in\mathbb{N}})$ of (2.4).

(ii) Moreover, for $G(u)\, f_i = \delta_{1i}\rho u$, where, $\{f_i\}$ is an orthonormal basis on K, there exists a positive deterministic function $\kappa : [1,\infty)\times(0,\infty) \to (0,\infty)$ defined by

$$\kappa(R,\rho^2) := \left(\frac{\rho^2}{4C_1}\right)^{2\delta(s_0)} \frac{1}{R}, \tag{2.9}$$

where C_1 is a constant and $\delta := \delta(s) = \frac{\epsilon}{s+\alpha-q}$, for $q>1$ and $\epsilon>0$ satisfying

$$\lim_{\rho^2\to\infty} \kappa(R,\rho^2) = \infty, \tag{2.10}$$

such that whenever $|A^{\frac{s_0}{2}}u_0|^2 \leq \kappa(R,\rho^2)$ P-a.s., then

$$P(T^\infty = \infty) \geq 1 - \frac{1}{R^{1/4}} \tag{2.11}$$

and

$$P\left(\lim_{t\to\infty} |A^{\frac{s_0}{2}}u(t)| = 0\right) \geq 1 - \frac{1}{R^{1/8}}. \tag{2.12}$$

Hence for multiplicative noise defined in Theorem 2.2.2(ii), (2.8) becomes,

$$u(t) = e^{-tA}g - \frac{1}{2}\int_0^t e^{-(t-s)A}\frac{\partial}{\partial x}u^2 ds + \int_0^t \rho u e^{-(t-s)A} dW(s), \tag{2.13}$$

2.2.1 The Limiting Cases

Theorem 2.2.2 asserts that, under the condition that $s_0 \geq 1$ and that $G(u) = \rho u$, the stochastic differential equation (2.7) admits a unique local solution that depends continuously on the initial conditions, almost surely. Additionally, the theorem establishes the existence of a maximal strong solution, indicating that there is a largest possible interval of existence——potentially infinite——over which the solution is well-defined. The solution of the stochastic problem (2.13) is a result of two inputs, namely, the initial condition g and the stochastic actuation with the magnitude controlled by the parameter ρ. Informally speaking, the theorem asserts that the probability of the solutions of problem (2.13) existing globally in time increases as the effect of the stochastic excitation becomes more significant relative to the "size" of the initial data, with the balance between the two parameters represented by the function $\kappa(R, \rho^2)$ in (2.9) The implication that $\lim_{t\to\infty} |A^{s_0/2}u(t)| = 0$ is highly probable suggests that the system is likely to stabilize to a state of minimal energy or fluctuation over time, assuming the initial conditions and noise intensity adhere to the bounds prescribed by $\kappa(R, \rho^2)$.

To explore implications of this theorem for blow-up phenomena under different conditions, we analyze the behavior of the function $\kappa(R, \rho^2)$. Given Theorem 2.3.1, we

have $s_0 > \frac{3}{2} - 2\alpha$ and for our problem we have $s_0 = 1$ [38]. Then, in the supercritical regime, i.e., for $\alpha \in (0, \frac{1}{2})$, we select $\alpha > \frac{1}{4}$. This also confirms [49] that α should be $\alpha > \frac{1}{4}$ to ensure the local well-posedness in H^1 for certain initial data in the deterministic case.

To fix attention, consider the case where $\alpha = \frac{3}{8}$ and $s_0 = 1$. This gives $\delta(s_0) > 0$ for $q > 1$ and $\varepsilon > 0$ [41], which generally occurs as long as q falls within the range $1 < q < 1 + \alpha$. Hence the following scenarios may occur:

1. For a fixed ρ and $R \to 0$:

   - Significant changes occur in the behavior of the function $\kappa(R, \rho^2)$ that sets the threshold for the squared norm $|A^{s_0/2}u_0|^2$ of the initial conditions. Specifically, $\kappa(R, \rho^2)$ increases without bound, suggesting that the restrictions on the initial conditions necessary to guarantee global existence and the decay property of the solution become less stringent. Practically, this implies that almost any initial condition could meet the requirement as R decreases.

   - In terms of the probability of global existence, denoted by $\mathbb{P}(T_\infty = \infty) \geq 1 - \frac{1}{R^{1/4}}$, it becomes undefined as R vanishes. This trend suggests a diminished confidence in the solution's persistence, indicating an increased likelihood of the solution blowing up or ceasing to exist within a finite time, particularly under very small R values.

2. For a fixed ρ and $R \to \infty$:

   - The upper bound set by $\kappa(R, \rho^2)$ on $|A^{s_0/2}u_0|^2$ becomes increasingly restrictive. This means that the initial conditions must be progressively

closer to zero for the bounds set by $\kappa(R, \rho^2)$ to be satisfied. Practically, this restricts the set of initial conditions that guarantee global existence and the decay property of the solution as stipulated by the theorem.

- The probability that the solution exists globally in time, $\mathbb{P}(T_\infty = \infty)$, is given by $1 - \frac{1}{R^{1/4}}$. As R grows, this probability approaches 1, indicating an increased confidence in the solution persisting indefinitely. This suggests a stronger likelihood of stability and a reduced chance of blow-up phenomena as R becomes significantly large. In particular, with the stochastic actuation of finite magnitude $\rho > 0$ and with the initial data of vanishing "size", solutions of problem (2.13) exist globally in time almost surely.

3. For a fixed R and $\rho \to \infty$:

   - The upper bound $\kappa(R, \rho^2)$ on $|A^{s_0/2} u_0|^2$ becomes large, effectively becoming unbounded. This indicates that the initial conditions could be increasingly large while still satisfying the requirements set by $\kappa(R, \rho^2)$ for global existence and decay of the solution. The practical implication is that the system can start from a broader range of initial states and still exhibit controlled behavior according to the theorem.

   - The practical effect of an unbounded κ suggests that there are fewer constraints on achieving global existence. In other words, as the noise magnitude increases, a given probability $\mathbb{P}(T_\infty = \infty)$ of global existence can be achieved for initial data of increasing "size".

In summary, while decreasing R relaxes the constraints on initial conditions, it also reduces the probability of global existence. Conversely, increasing R enhances the

probability of a global existence of solutions but necessitates smaller initial conditions. Furthermore, an increase in ρ directly contributes to the system's ability to handle larger initial conditions, thus reducing the likelihood or delaying the onset of blow-up.

We define $\mathcal{E}_0 := \|u_0\|_{H^1}$, which is subject to the inequality:

$$\mathcal{E}_0 < \kappa(R, \rho^2) \approx O\left(\frac{1}{R}\right) \text{ as } R \to \infty,$$

indicating that as R increases, the upper bound on $\mathcal{E}_0$ becomes more stringent, approaching zero.

Upon replacing R with $\mathcal{E}_0^{-1}$, we observe:

$$P(T_\infty = \infty) \geq 1 - \mathcal{E}_0^{1/4}, \quad \text{for} \quad \mathcal{E}_0 \ll 1,$$

This substitution simplifies the analysis by directly relating $\mathcal{E}_0$, a measure of the "size" of the initial condition, to the probability of the solution existing globally.

Objective of this Work: The primary goal of this work is to illustrate these theoretical predictions numerically. By conducting comprehensive numerical experiments, we aim to quantify the effects of varying R and ρ on the global existence of solutions. Since in this work we considered, a fixed initial data $g(x) = \sin(x)$ this allows us to explore how changes in ρ impact the persistence of solutions. This numerical analysis not only serves to validate the theoretical insights but also provides practical guidance on parameter selection for ensuring desired system behaviors in stochastic differential equations.

2.3 Diagnostic Quantities

Two quantities that will be used to characterize the behavior of the solutions, namely whether or not these solutions blow up, are the width of analyticity strip, δ and the enstrophy, $\mathcal{E}$.

Firstly, in case of deterministic system (2.1), the enstrophy, denoted $\mathcal{E}(t)$, is computed as follows:

$$\mathcal{E}(t) := \pi \int_0^{2\pi} \left| \frac{\partial u(t,x)}{\partial x} \right|^2 dx, \tag{2.13}$$

For the stochastic system (2.4) the enstrophy, denoted as $\mathcal{E}_\omega(t)$, is computed pathwise, that is for each $\omega \in \Omega$

$$\mathcal{E}_\omega(t) := \pi \int_0^{2\pi} \left| \frac{\partial u(t,x;\omega)}{\partial x} \right|^2 dx, \ \omega \in \Omega \tag{2.14}$$

This expression remains well-defined because the function $u(t,\cdot;\omega)$ belongs to the space $H^1([0,2\pi])$ for all time $t \in [0,\tau]$, as established in Theorem 2.2.2. On the other hand, the blowup of an individual realization of the stochastic process $u(t,x,\omega)$ is signalled by an unbounded growth of $\mathcal{E}_\omega(t)$ for $t > \tau$.

Using (2.14), we introduce the "stopping time", denoted as $\tilde{\tau}_R$, and the corresponding "maximum existence time," denoted T^∞. These are defined similarly to the quantities introduced in Definition 2.2.1 and expressed as follows [41]:

$$\widetilde{\tau}_R(\omega) := \inf\{t > 0 : \mathcal{E}_\omega(t) \geq R\}, \quad R \in \mathbb{N}, \tag{2.15}$$

$$T^{\infty} := \lim_{R \to \infty} \tilde{\tau}_R \tag{2.16}$$

It is important to note that when dealing with zero-mean functions the space $H^1([0, 2\pi])$, the expression for enstrophy in (2.13) is equivalent to the H^1 norm. As a result, the maximum existence time T^{∞} defined in Definition 2.2.1 aligns with the concept introduced in (2.16). This allows us to compute T^{∞} by means of (2.15).

Furthermore, it is worth mentioning that the maximum existence time in the context of system (2.4) is as a random variable, characterized by a specific distribution $T^{\infty} = T^{\infty}(\omega)$, $\omega \in \Omega$. The determination of this distribution forms an integral part of solving the problem at hand.

Secondly, the width of the analyticity strip at a time t, $\delta(t)$, is defined as the distance from the nearest complex singularity in the complex extension of the solution at the time t to the real axis. To understand the importance of this quantity, let us recall the following theorem from [44]:

Theorem 2.3.1. *(Paley-Weiner Theorem) Let $u \in L^2(\mathbb{R})$ have Fourier Transform $\mathcal{F}[u] = \widehat{u}$. Suppose there exist $\delta, \delta_1 > 0$ such that u can be extended to an analytic function in the complex strip $|\operatorname{Im}(z)| < \delta$ with $\|u(\cdot + iy)\|_2 \leq \delta_1$ uniformly for all $y \in (-\delta, \delta)$, where $\|u(\cdot + iy)\|_2 \leq \delta_1$ is the L^2 norm along the horizontal line $\operatorname{Im}(z) = y$. Then $u_\delta \in L^2(\mathbb{R})$, where $u_\delta(k) = e^{\delta|k|}\widehat{u}(k)$ for $k \in \mathbb{R}$. The converse also holds.*

The results of Theorem 2.3.1 also extend to functions defined on periodic domains. The maximum value of δ in Theorem 2.3.1 represnts the width of the analyticity strip of $u(t, x)$. In the context of problem (2.1), a solution loses its analyticity when the singularities, present in its extension into the complex plane collapse onto the x-axis, leading to the vanishing of the width of the analyticity strip $\delta(t)$. In other words,

the solution experiences a blow-up. As solutions of the stochastic system (2.4) are generally not analytic in x, the width of the analyticity strip cannot be used to characterize their regularity.

Chapter 3

Numerical Approach

In this chapter we delve into the numerical methodologies employed to explore the properties of the fractional Burgers equation in both the deterministic and stochastic setting. The chapter begins by introducing the solution approach for the deterministic model, focusing on numerical methods that replicate theoretical behaviors accurately in the absence of stochastic actuation. It then progresses to include stochastic components that reflect the uncertainty of the systems. The deterministic analysis provides a foundational understanding, establishing a baseline against which the effects of stochastic variables are evaluated.

3.1 Deterministic Fractional Burgers Equation

In the numerical solution of system (2.1), we utilized the Fourier-Galerkin pseudo-spectral method suitable for the periodic boundary conditions. The solution is approximated by a finite sum of Fourier modes:

$$u_N(t,x) = \sum_{k=-N/2+1}^{N/2} \widehat{u}_k(t) e^{ikx}, \tag{3.1}$$

where $\widehat{u}_k(t)$ represents the Fourier coefficients of $u(t,x)$, computed as:

$$\widehat{u}_k(t) = \frac{1}{2\pi} \int_0^{2\pi} u(t,x) e^{-ikx} dx. \tag{3.2}$$

For an efficient computation of the Fourier coefficients, $N = 2^n$ (where $n \in \mathbb{N}$) is chosen to be a power of 2. The solutions are real-valued functions, so only half of the Fourier modes are computed due to the conjugate symmetry, i.e., $\widehat{u}_{-k} = \overline{\widehat{u}_k}$, $k \in \mathbb{Z}$. Additionally, we ensure that $\widehat{u}_0(t) = 0$ at all times to maintain the zero-mean property (cf. equation (2.1.1)). Substituting equation (3.1) into system (2.1) yields an ODE system:

$$\frac{d\widehat{\mathbf{u}}}{dt} = \mathbf{r}(\widehat{\mathbf{u}}(t)) + \mathbf{A}\widehat{\mathbf{u}}(t), \tag{3.3a}$$

$$\widehat{\mathbf{u}}(0) = \widehat{\mathbf{g}}, \tag{3.3b}$$

where $\widehat{\mathbf{u}}(t)$ and $\widehat{\mathbf{g}}$ are vectors of the Fourier coefficients at time t and the initial condition, respectively. The operators $\mathbf{r}$ and $\mathbf{A}$ map from $\mathbb{C}^{N/2}$ to $\mathbb{C}^{N/2}$, with their

k-th components defined as:

$$[\mathbf{r}(\widehat{\mathbf{u}}(t))]_k = -\frac{1}{2}ik[\widehat{u^2}(t)]_k,$$
$$[\mathbf{A}\widehat{\mathbf{u}}(t)]_k = -\kappa k^2 \widehat{u}_k(t),$$

for $k = 1, \ldots, N/2$, where $\widehat{u^2}(t)$ denotes the Fourier coefficients of the function $u^2(t, x)$. The Fast Fourier Transform (FFT) is employed for the computation of Fourier coefficients, and the "3/2 rule" of dealiasing is employed in spectral methods to prevent aliasing errors during nonlinear operations, such as convolutions. Initially, the spectral representation of a function is padded to extend the number of modes to 3/2 times the original number, effectively preventing high-frequency components from wrapping around and causing aliasing. Nonlinear operations are performed in this extended spectral space, and the result is then truncated back to the original number of modes, eliminating potential aliasing errors. This technique ensures more accurate numerical solutions by mitigating the impact of aliasing in spectral methods.

The temporal integration is performed using a hybrid method combining Crank-Nicolson (CN) and a three-step Runge-Kutta (RK) method. The numerical scheme is:

$$\left(\mathbf{I} - \frac{h_{rk}}{2}\mathbf{A}\right)\widehat{\mathbf{u}}_{rk+1} = \widehat{\mathbf{u}}_{rk} + \frac{h_{rk}}{2}\mathbf{A}\widehat{\mathbf{u}}_{rk} + h_{rk}\phi_{rk}\mathbf{r}(\widehat{\mathbf{u}}_{rk}) + h_{rk}\psi_{rk}\mathbf{r}(\widehat{\mathbf{u}}_{rk-1}), \tag{3.4}$$

where $rk = 1, 2, 3$, and the constants are defined as $h_1 = \frac{8}{15}\Delta t$, $h_2 = \frac{2}{15}\Delta t$, $h_3 = \frac{1}{3}\Delta t$, $\phi_1 = 1$, $\phi_2 = \frac{25}{8}$, $\phi_3 = \frac{9}{4}$, $\psi_1 = 0$, $\psi_2 = -\frac{17}{8}$, $\psi_3 = -\frac{5}{4}$. In this scheme, $\hat{\mathbf{u}}_1$ and $\hat{\mathbf{u}}_4$ represent the solutions of system (3.3) at the current and future time, respectively. In the context of the Runge-Kutta integration method, the steps $\widehat{\mathbf{u}}_2$ and

$\widehat{\mathbf{u}}_3$ serve as intermediary calculations. We will be referring to this numerical method as CNRK3. Important features to highlight concerning the numerical method (3.4) are an explicit and an implicit treatment of the nonlinear and linear part of equation (3.3a), respectively. Deduction of the numerical method can be found in [6]. The order of convergence of the CNRK3 method is two, which is the order of convergence of the less accurate method between CN and RK3. As regards stability, we require the time step to be small enough, i.e., we will ask that

$$\Delta t \leq C(\Delta x)^{\eta}; \tag{3.5}$$

where C is a constant, $\eta \in \{1, 2\}$, and Δt and Δx are the grid sizes in time and space, respectively. Here, $\eta = 1$. Our objective includes accurately approximating solutions of system (2.1), particularly in the supercritical region close to the blow-up time. For this, a substantial number of Fourier coefficients, is essential. Nonetheless, starting the solution of the partial differential equation with a high resolution from the outset is not efficient. In the initial stages, especially with smooth initial conditions, only a few Fourier coefficients accurately resolve the solution. To address this, an automatic grid refinement strategy is implemented [38]. As the solution develops, the resolution N is initially set low and doubled progressively based on an analysis of the Fourier coefficients. If these coefficients do not exhibit exponential decay—signifying an under-resolve solution—a refinement is triggered. To prevent the accumulation of round-off errors, a sharp low-pass filter is applied to discard Fourier coefficients below a machine precision threshold of 10^{-17}. The spatial and temporal grid sizes ($\Delta x = \frac{2\pi}{N}$ and $\Delta t = O\left(\frac{1}{N}\right)$, respectively) are adjusted dynamically until the spectrum's resolution is deemed adequate.

Using Parseval's identity and representation (3.1), the enstrophy (2.13) is approximated as [38]

$$\mathcal{E}(t) \approx 4\pi^2 \sum_{k=1}^{N/2} k^2 |\widehat{u}_k(t)|^2. \tag{27}$$

Regarding the width of the analyticity strip $\delta(t)$, we adopt the methodology from the classical paper [42]. Assuming the extension of the solution $u(t,\cdot)$ into the complex plane has its nearest singularity at $z_j \in \mathbb{C}$, where $\mathrm{Im}(z_j) = \delta$, as stated in Theorem 2.3.1, and near this singularity the solution behaves as

$$u(z) \sim (z - z_j)^{\eta},$$

it can be shown using Laplace's method that the Fourier spectrum of $u(t,.)$ admits the following asymptotic representation

$$|\widehat{u}_k| \sim C k^{-(1+\eta)} e^{-\delta k}, \text{ for } k \to \infty, \tag{28}$$

where C is a scaling parameter. An estimate of $\delta = \delta(t)$ can then be obtained by minimizing the least-squares error between this representation and the amplitudes of the Fourier coefficients $|\widehat{u}_1(t)|, \ldots, \left|\widehat{u}_{N/2}(t)\right|$.

3.2 Stochastic Fractional Burgers Equation

We will be using the Euler-Maryama method (EM) and Milstein method (MIL) to study system (2.13). A Monte Carlo method was selected to sample noise primarily because of its well-documented convergence behavior and ease of implementation. While newer techniques, such as polynomial chaos expansions, could theoretically offer

more rapid convergence, their implementation complexity and higher computational demands make them less practical. Furthermore, representing the nonlinear term in a polynomial orthonormal basis introduces significant complexity, as discussed in [32]. It is also noteworthy that the time-invariant structure of the noise characteristics in the model equations (2.5)–(2.6) means that grid refinement is unnecessary for accurately resolving the stochastic model, as the required resolution does not vary over time.

3.2.1 Euler-Maruyama Method (EM)

We will consider a Fourier representation of the solution as in expression (3.1). Again, the conjugate symmetry property holds and only functions with mean zero are considered. Now, plugging expression (3.1) in equation (2.13), we obtain

$$d\widehat{\mathbf{u}} = (\mathbf{r}(\widehat{\mathbf{u}}(t)) + \mathbf{A}\widehat{\mathbf{u}}(t))dt + \rho\widehat{\mathbf{u}}(t)d\mathbf{W}(t), \quad \widehat{\mathbf{u}}(0) = \widehat{\mathbf{g}}, \tag{3.6}$$

where $\widehat{\mathbf{u}}(t)$, $\mathbf{r}(\widehat{\mathbf{u}}(t))$ and $\mathbf{A}\widehat{\mathbf{u}}$ are as in system (3.3) and $\mathbf{W}(t) = [W_1(t), \ldots, W_{N/2}(t)]^T$, where

$$W_k(t) = \frac{\sqrt{2}}{2k}(\beta_{2k}(t) - i\beta_{2k-1}(t)), \ k = 1, 2, ... \tag{3.7}$$

and $\beta_1, \ldots, \beta_N$ are i.i.d standard Brownian motions. According to [37], (3.7) ensures that the noise $W(t)$ is square-integrable in L^2 for all times which in turn guarantees that the mild solution (2.13) of the system (3.6) is well defined in H^1.

Following the same idea as in the numerical approach to the deterministic version of the fractional Burgers equation, we will use the FFT to compute the Fourier coefficients. We will also use the "3/2 rule" to avoid the aliasing phenomenon. For a

time step $\Delta t > 0$ and initial condition $\widehat{\mathbf{u}}_0 \in \mathbb{R}^d$, the Euler–Maruyama approximation $\widehat{\mathbf{u}}_n$ to the solution $\widehat{u}(t_n)$ of (3.6) for $t_n = n\Delta t$ is defined by

$$\widehat{\mathbf{u}}_{n+1} = \widehat{\mathbf{u}}_n + f(\widehat{\mathbf{u}}_n)\Delta t + G(\widehat{\mathbf{u}}_n)\Delta W_n, \tag{3.8}$$

where $\widehat{\mathbf{u}}_n$ stands for the solution of system (3.6) at the n-th time step, Δt is the size of the time step, $f(\widehat{\mathbf{u}}) = \mathbf{r}(\widehat{\mathbf{u}}(t)) + \mathbf{A}\widehat{\mathbf{u}}(t)$, $G(\widehat{\mathbf{u}}) = \rho\widehat{\mathbf{u}}(t)$ and $\Delta W_n = W_{n+1} - W_n$, where W_n is the noise at the n-th time step. To compute ΔW_n, we use the expression

1. Consider $\boldsymbol{\xi}$ as independent $\mathbb{C}^{N/2}$-valued Gaussian variables with distribution $\mathcal{N}(0, I_{N/2})$, where $I_{N/2}$ is the identity matrix of size $N/2 \times N/2$.

2. Set $\Delta W_n = \sqrt{\Delta t}\,\boldsymbol{\xi}$

3.2.2 Milstein Method (MIL)

The Milstein method has a higher order of convergence compared to the Euler-Maruyama method [32], $\widehat{\mathbf{u}}_n$ to the solution $\widehat{u}(t_n)$ of (3.6) for $t_n = n\Delta t$ is defined by

$$\widehat{u}_{k,n+1} = \widehat{u}_{k,n} + f_k(\widehat{\mathbf{u}}_n)\Delta t + g_{kk}(\widehat{\mathbf{u}}_n)\Delta W_{k,n} + \frac{1}{2}\frac{\partial g_{kk}}{\partial \widehat{\mathbf{u}}_k}(\widehat{\mathbf{u}}_n)g_{kk}(\widehat{\mathbf{u}}_n)\left(\Delta W_{k,n}^2 - \Delta t\right) \tag{3.9}$$

where $\Delta W_{i,n} = \left(\int_{t_n}^{t_{n+1}} dW_i(r)\right)$, and $\widehat{u}_{k,n}$ is the k-th component of $\widehat{\mathbf{u}}_n$. Here $G(\widehat{\mathbf{u}}_n)$ has the k-th component g_{kn}, $f(\widehat{\mathbf{u}}_n)$ has the k-th component, f_k. Also, it is supposed that the noise is diagonal (i.e., G is a diagonal matrix), i.e., each component u_k is

affected by W_k only, as $g_{kj} = 0$ when $j \neq k$. Also, The noise is commutative when

$$\frac{\partial g_{kj}}{\partial \widehat{u}_l} g_{li} = \frac{\partial g_{ki}}{\partial \widehat{u}_l} g_{lj}, \tag{3.10}$$

for any indices i, j, k, l. The commutativity condition implies that the order in which these operations are computed does not affect the outcome, reducing the potential for error accumulation in the numerical integration process.

3.3 Validation of the Methods

Here, we compare the results of Euler-Maryama method and Milstein method in the subcritical case. The methods are employed with the following parameters: the fractional exponent $\alpha = 0.9$, the resolution $N = 2^8$, initial condition $g(x) = \sin(x)$ and the viscosity $\nu = 0.11$ for different values of ρ. To compare the results, the statistical moments of $\mathcal{E}_\omega^{max}$ are analyzed, keeping the spacial and temporal discritization fixed and varying the discritization of the probability space. Here, the stability and convergence of a method can depend heavily on how the noise is discretized and that is why only the discritization of the probability space is allowed to vary. To recall, the initial four statistical moments of a random variable X, specifically, the mean μ denoted as $E[X]$, variance σ^2 denoted as $E[(X-\mu)^2]$, skewness S denoted as $E\left[\left(\frac{X-\mu}{\sigma}\right)^3\right]$, and kurtosis K denoted as $E\left[\left(\frac{X-\mu}{\sigma}\right)^4\right]$, where $E[\cdot]$ represents the expectation as defined earlier, are computed for the maximum attained enstrophy defined as, $\mathcal{E}_\omega^{\max} := \max_{t\geq 0} \mathcal{E}_\omega(t)$ acquired under varying noise amplitudes ρ in the subcritical case. We focus here on

the subcritical regime. A approximation of these moments are constructed as follows:

$$\text{Mean } (\mu) \approx \mu_m := \frac{1}{m}\sum_{\omega=1}^{m} \mathcal{E}_{\omega}^{\max} \tag{3.11.a}$$

$$\text{Variance } (\sigma^2) \approx \sigma_m^2 := \frac{1}{m}\sum_{\omega=1}^{m} (\mathcal{E}_{\omega}^{\max} - \mu_m)^2 \tag{3.11.b}$$

$$\text{Skewness } (S) \approx S_m := \frac{1}{m}\sum_{\omega=1}^{m} \left(\frac{\mathcal{E}_{\omega}^{\max} - \mu_m}{\sigma_m}\right)^3 \tag{3.13.c}$$

$$\text{Kurtosis } (K) \approx K_m := \frac{1}{m}\sum_{\omega=1}^{m} \left(\frac{\mathcal{E}_{\omega}^{\max} - \mu_m}{\sigma_m}\right)^4 \tag{3.11.d}$$

Here, the number of samples, m ranges from 1 to M, notation of the number of samples used for the approximations, and $\{\mathcal{E}_{\omega}^{\max}\}, \omega = 1, .., M$ is the maximum enstrophy value attained in the ωth realization. Here M=10000 is the total number of samples used.

We compare these approximations to the normal (Gaussian) distribution given by the expression

$$f(\mathcal{E}_{\omega}^{\max}, \mu, \sigma) = \frac{1}{\sqrt{2\pi}\sigma} \exp\left(-\frac{(\mathcal{E}_{\omega}^{\max} - \mu)^2}{2\sigma^2}\right), \tag{3.11.e}$$

where μ is the mean and σ is the standard deviation of a certain set of samples.

Figure 3.1 illustrates the PDF of maximum enstrophy derived from simulations using the Euler-Maryama method and the Milstein method. Both the distributions show a pronounced peak with tails tapering off symmetrically, characteristic of the Gaussian distribution. This suggests that the stochastic processes governing enstrophy dynamics, despite their complexity, conform to the Central Limit Theorem (CLT). The theorem posits that a mean of a large number of small, independent disturbances

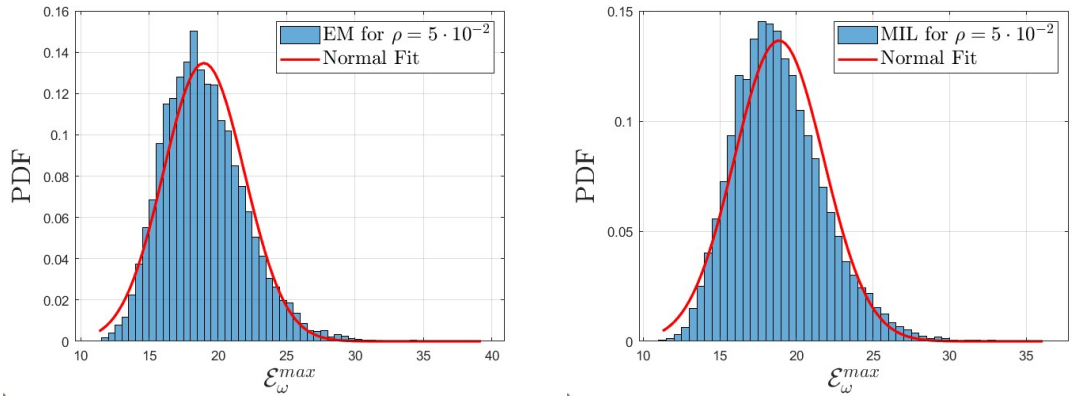

Figure 3.1: PDF of the maximum enstrophy $\mathcal{E}_\omega^{\max}$ for (a) EM and (b) MIL with $\rho = 5 \cdot 10^{-2}$

tends to exhibit normal distribution, assuming identically distributed independent increments. The absence of non-Gaussian features implies that these conditions are effectively met, indicating the simulations lack significant skew or extreme events that might disrupt this behavior. Additionally, the similarity in distributions obtained from both numerical methods underscores their reliability and suggests that numerical settings, like discretization, do not adversely affect the observed statistical properties. This consistency is crucial for validating these methods for studying the system's statistical dynamics.

In the analysis of the mean enstrophy μ_m in Figure 3.2 the Milstein method exhibits lower values across the simulations when compared to the Euler-Maruyama method, demonstrating less sensitivity to the increase in ρ. Notably, the reduced fluctuation in mean enstrophy with the Milstein method suggests that it may reach a stable solution with fewer samples, enhancing computational efficiency. Also, Figure 3.2c suggests that for lower noise magnitude $\rho = 7 \cdot 10^{-4}$ the mean from both methods may converge for sufficiently large samples. The ability of the Milstein method

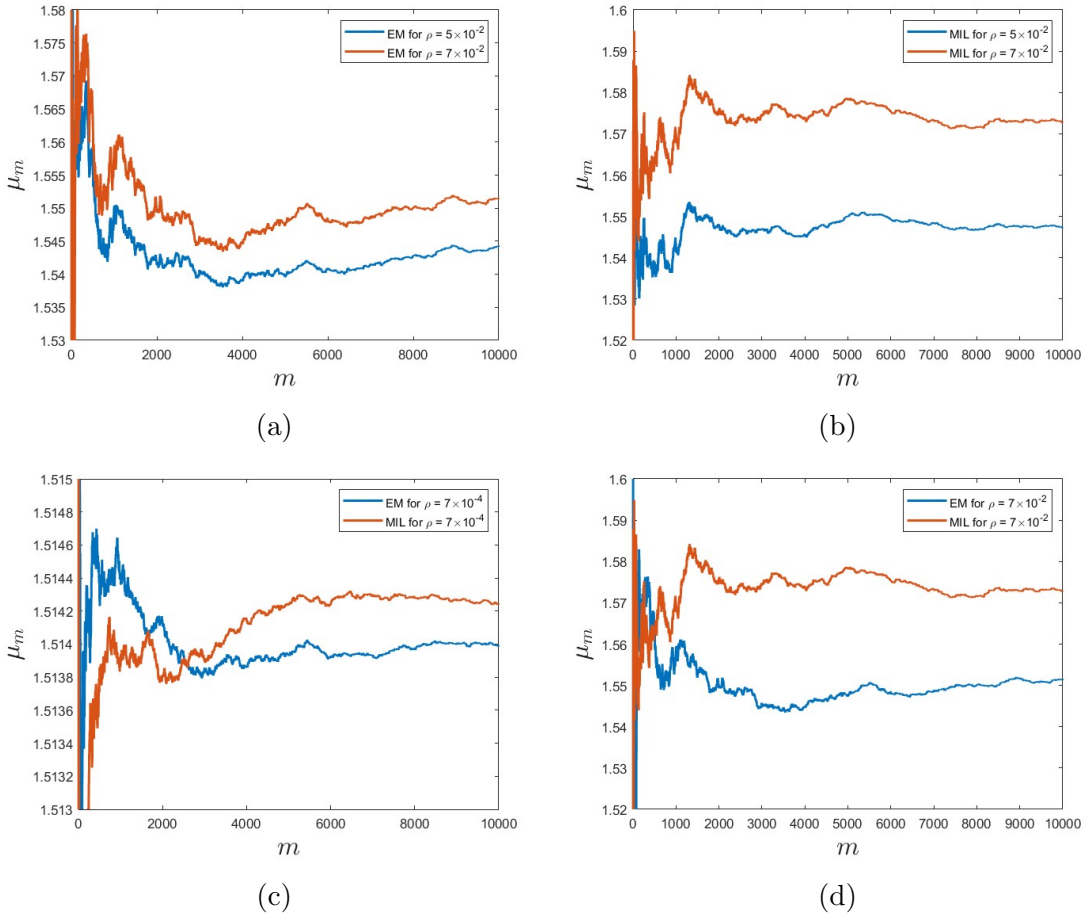

Figure 3.2: Mean of maximum enstrophy $\mathcal{E}_\omega^{\max}$ for different simulations: (a) EM method with $\rho = 5 \cdot 10^{-2}$ and $\rho = 7 \cdot 10^{-2}$, (b) MIL method for $\rho = 5 \cdot 10^{-2}$ and $\rho = 7 \cdot 10^{-2}$, (c) comparison of both methods with a lower noise intensity $\rho = 7 \cdot 10^{-4}$, and (d) comparison of both methods for a higher noise intensity $\rho = 7 \cdot 10^{-2}$.

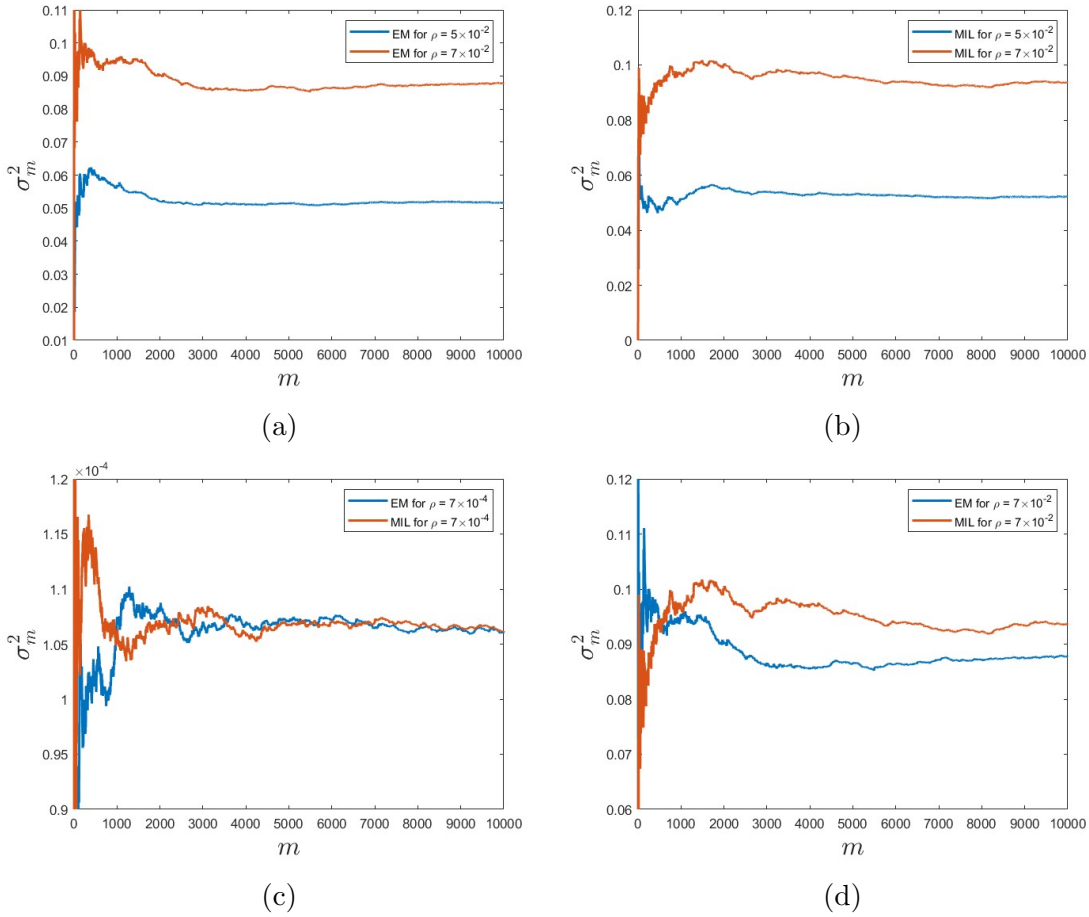

Figure 3.3: Varience of maximum enstrophy $\mathcal{E}_\omega^{\max}$ across different simulations: (a) EM method with $\rho = 5 \cdot 10^{-2}$ and $\rho = 7 \cdot 10^{-2}$, (b) MIL method for $\rho = 5 \cdot 10^{-2}$ and $\rho = 7 \cdot 10^{-2}$, (c) comparison of both methods with a lower noise intensity $\rho = 7 \cdot 10^{-4}$, and (d) comparison of both methods for a higher noise intensity $\rho = 7 \cdot 10^{-2}$.

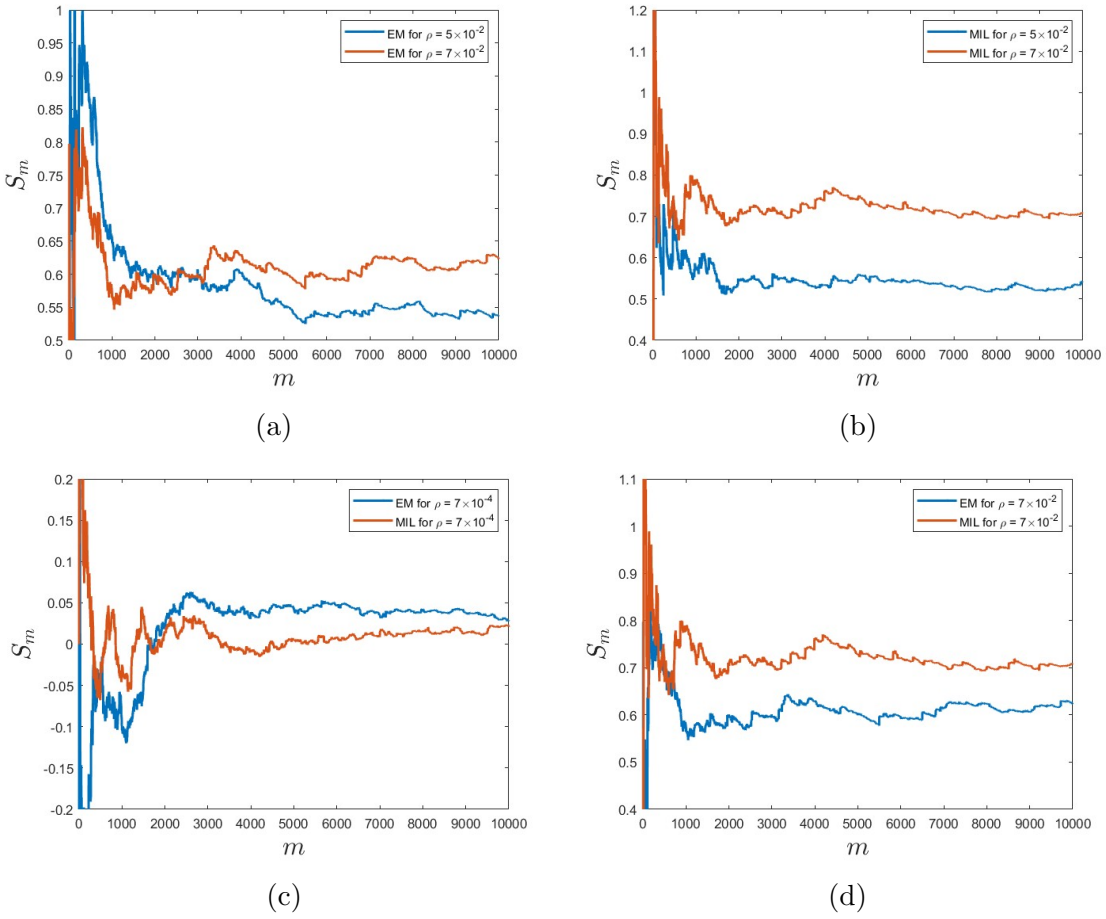

Figure 3.4: Skewness of maximum enstrophy $\mathcal{E}_\omega^{\max}$ for different simulations: (a) EM method with $\rho = 5 \cdot 10^{-2}$ and $\rho = 7 \cdot 10^{-2}$, (b) MIL method for $\rho = 5 \cdot 10^{-2}$ and $\rho = 7 \cdot 10^{-2}$, (c) comparison of both methods with a lower noise intensity $\rho = 7 \cdot 10^{-4}$, and (d) comparison of both methods for a higher noise intensity $\rho = 7 \cdot 10^{-2}$.

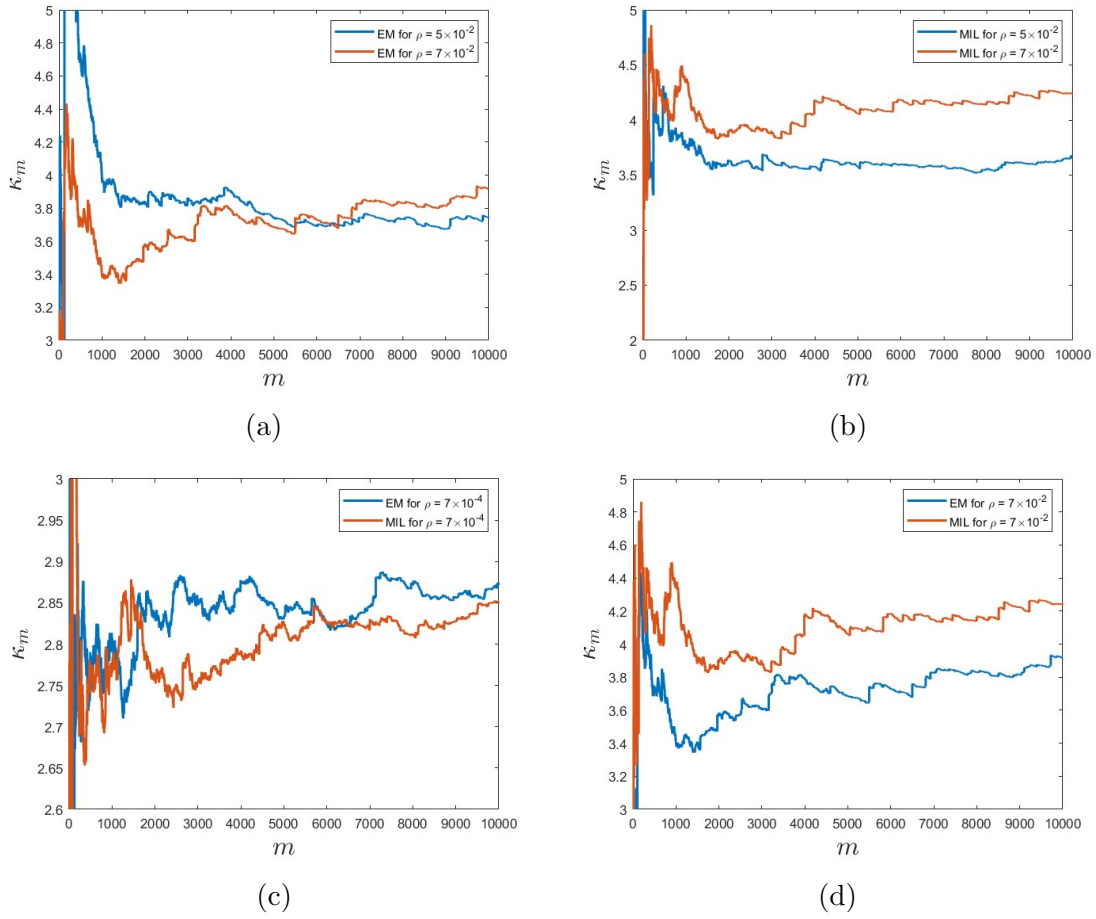

Figure 3.5: Kurtosis of maximum enstrophy $\mathcal{E}_\omega^{\max}$ across different simulations: (a) EM method with $\rho = 5 \cdot 10^{-2}$ and $\rho = 7 \cdot 10^{-2}$, (b) MIL method for $\rho = 5 \cdot 10^{-2}$ and $\rho = 7 \cdot 10^{-2}$, (c) comparison of both methods with a lower noise intensity $\rho = 7 \cdot 10^{-4}$, and (d) comparison of both methods for a higher noise intensity $\rho = 7 \cdot 10^{-2}$.

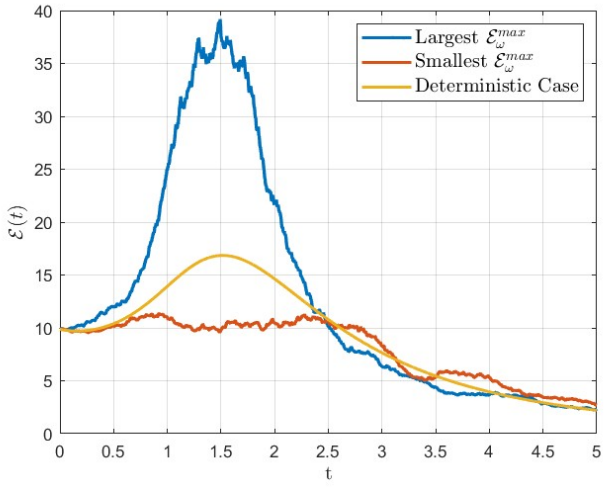

Figure 3.6: The time evolutions of the enstrophy in the stochastic realizations characterized by the largest and smallest values of $\mathcal{E}_\omega^{\max}$ for $\rho = 5 \cdot 10^{-2}$ with the deterministic case.

to produce solutions with a potentially reduced number of samples could translate into significant savings in computational time and cost, along with maintaining high accuracy in the presence of stochastic perturbations.

The variance of enstrophy σ_m^2 reveals crucial differences between the Euler-Maruyama and Milstein methods in Figure 3.3. A larger variance observed with the Euler-Maruyama method, especially at increased noise intensities ρ, may not only indicate greater system fluctuations but also raises questions about the sample size adequacy for variance estimation. A sufficient sample size is critical to ensure that the calculated variance is an acurate estimator of the system's actual variability. The Milstein method displays a notably lower variance, suggesting not only its higher accuracy but also potentially implying its efficiency in achieving statistically reliable variance estimates with a smaller sample size. This efficiency of the Milstein method makes it preferable in scenarios where computational resources are limited or when a high

number of simulations are required for a thorough exploration of the system's behavior.

The analysis of skewness (S_m), as depicted in Figures 3.4, offers insights into the asymmetry of the enstrophy distribution under different noise intensities (ρ). Figure 3.4a reveals that the Euler-Maruyama method exhibits lower skewness for higher ρ values, suggesting an initial prevalence of lower enstrophy values and hinting at a potential bias in the early phase of the simulation. As the simulation progresses, the skewness metric gradually trends towards zero, indicative of the distribution's movement toward symmetry around the mean enstrophy. On the contrary, the Milstein method, as shown in Figure 3.4b, demonstrates relatively consistent skewness from the outset, which persists across the simulation time. This consistency is indicative of the method's ability to maintain symmetry in the distribution of enstrophy values and implies a stable simulation process. The less variable skewness observed with the Milstein method from Figure 3.4c and Figure 3.4d may also suggest that a smaller sample size is sufficient to achieve an accurate representation of the system's behavior, thus enhancing computational efficiency.

Figures 3.5 provide a analysis of the kurtosis of the maximum enstrophy (K_m) for the Euler-Maruyama and Milstein methods under varying noise intensities, $\rho = 5{\cdot}10^{-2}$ and $\rho = 7{\cdot}10^{-2}$, respectively. Notably, the Euler-Maruyama method exhibits an initial spike in kurtosis particularly for the larger value of ρ, hinting at a higher likelihood of extreme enstrophy outcomes early in the simulation. As the number of samples m increases, the kurtosis for both levels of noise intensity diminishes, suggesting a regression of enstrophy distribution towards that of a normal distribution. This convergence towards a normal distribution indicates that the initial extremes may be

transient and that the system's dynamics become more stable over time.

Figure 3.6 illustrates the enstrophy $\mathcal{E}_\omega^{\max}(t)$ as a function of time t, comparing stochastic simulations using the Milstein method with a deterministic case. The solid lines represent the realizations achieving the largest and smallest maximum enstrophy values $\mathcal{E}_\omega^{\max}$ obtained from an ensemble of stochastic simulations at noise intensity $\rho = 5 \cdot 10^{-2}$, while the dashed line denotes the enstrophy trajectory of the deterministic system. The stochastic results, bounded between maximum of $\mathcal{E}_\omega^{\max}$ and minimum of $\mathcal{E}_\omega^{\max}$, reflect the variability in the system's enstrophy due to the random perturbations, in contrast to the deterministic scenario which follows a single, noise-free trajectory. In the context of the Milstein method, the graph demonstrates that while the stochastic system exhibits a broader range of behaviors due to noise, the overall trend in enstrophy over time remains consistent with the deterministic case.

Together, these figures provide a comprehensive statistical understanding of the system dynamics under stochastic influence. The higher noise intensity leads to more variable and extreme enstrophy values initially, but as the a larger number of samples is accumulated, this variability is mitigated. Across all statistical measures, the Milstein method outperforms the Euler-Maruyama method, especially at higher noise levels, suggesting its suitability for systems where accurate representation of the noise influence is critical. These findings underscore the importance of choosing an appropriate numerical method for solving SDEs in the presence of significant stochastic forces, such as those investigated in the fractional Burgers equation.

Chapter 4

Results

It is important to emphasize that, while our primary focus is on the stochastic case, we begin by presenting the deterministic case as a reference. The deterministic scenario serves as a baseline, allowing us to understand the underlying dynamics without the influence of randomness. By first examining the deterministic case, we can establish a clear framework for the behavior of the system under controlled conditions. This foundation is crucial for highlighting the deviations and effects introduced by stochastic elements when we later analyze the stochastic case. Hence, the deterministic analysis provides essential insights that aid in the interpretation and contextualization of the results obtained from the stochastic simulations.

4.1 Deterministic Case

Building upon the insights from Section 2.1, this study focuses on the deterministic problem (2.1) across different regimes: in the subcritical regime we set α= 0.9, and in the supercritical regime α=0.4. The initial condition and viscosity are $g(x) = \sin(x)$

and $\nu = 0.11$. To solve this problem, the CNRK3 method, as outlined in Section 3.1, is employed. This approach features an adaptive resolution ranging from $N = 2^9$ to $N = 2^{18}$ in the supercritical scenario, and from $N = 2^9$ to $N = 2^{22}$ in the subcritical context.

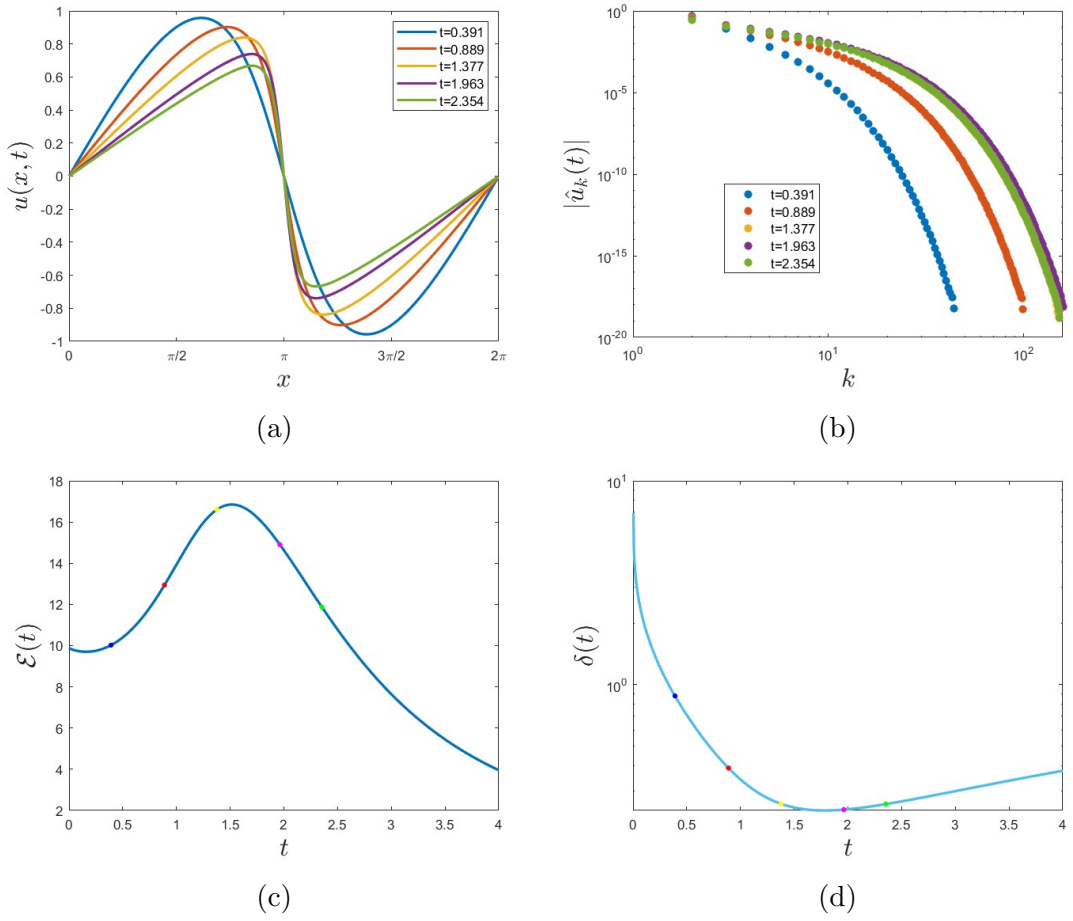

Figure 4.1: Solution of system (2.1) with $\alpha = 0.9$ in (a) the physical space $u(t, x)$ and (b) the Fourier space $|\hat{u}_k(t)|$ at the indicated time levels with the corresponding evolution of (c) the enstrophy $\mathcal{E}(t)$ and (d) the width of the analyticity strip $\delta(t)$. The symbols in panel (c) and (d) correspond to the time instances at which the solution is shown in panels (a) and (b).

In Figures 4.1 and 4.2, the dynamics of the solution in both physical and Fourier

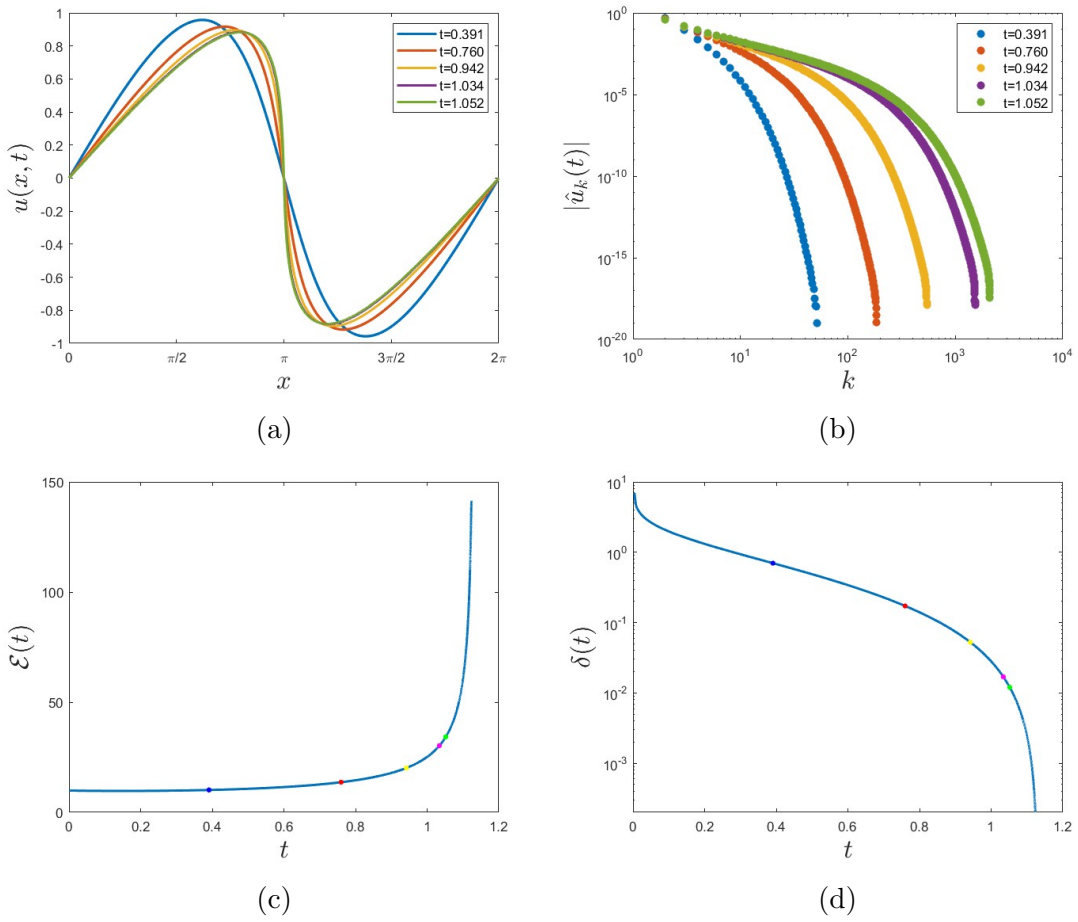

Figure 4.2: Solution of system (2.1) with $\alpha = 0.4$ in (a) the physical space $u(t, x)$ and (b) the Fourier space $|\hat{u}_k(t)|$ at the indicated time levels with the corresponding evolution of (c) the enstrophy $\mathcal{E}(t)$ and (d) the width of the analyticity strip $\delta(t)$. The symbols in panel (c) and (d) correspond to the time instances at which the solution is shown in panels (a) and (b).

spaces, alongside the enstrophy and the width of the analyticity strip, are illustrated. Figure 4.1 is associated with the subcritical regime, while Figure 4.2 represents the supercritical regime. The interplay between dissipative and nonlinear elements in system (2.1) is showcased in the physical space via Figures 4.1a and 4.2a. In Figure 4.1a, the early stages are characterized by the dominance of the nonlinear component, leading to an intensification of the solution's front. However, as time progresses, the dissipative term becomes more influential, resulting in the flattening of the front. In contrast, Figure 4.2a highlights the dominating effect of the nonlinear term in equation (2.1a), which induces the formation of shocks and subsequent finite-time singularities.

The Fourier space representations are detailed in Figures 4.1b and 4.2b. Figure 4.1b indicates that a limited number of Fourier coefficients are adequate for resolving problem (2.1) in the subcritical regime. On the other hand, Figure 4.2b shows that in the supercritical regime an increasing number of Fourier coefficients becomes necessary as time progresses. The enstrophy, as depicted in Figures 4.1c and 4.2c, behaves as anticipated: it remains bounded for smooth solutions and becomes unbounded when a singularity occurs at the blow-up time. Lastly, the width of the analyticity strip, shown in Figures 4.1d and 4.2d, reveals the emergence of a singularity in the supercritical case and remaining above zero for smooth solutions.

4.2 Stochastic Case

In this section, we examine the stochastic problem (2.7) in the supercritical regime with $\alpha = 0.4$. The initial condition and viscosity are kept as previously defined, with $g(x) = \sin(x)$ and $\nu = 0.11$. A fixed resolution of $N = 2^{14}$ is employed. Our focus is

on investigating the impact of the noise amplitude ρ on the estimates of the blow-up time, particularly in terms of deviations from the deterministic case. Since the blow-up time is a stochastic variable characterized by a certain probability distribution, it will be described appropriately. As mentioned in Section 2.3, due to the lack of analyticity in the solution caused by the noise, we will use enstrophy exclusively to estimate the blow-up time.

We use a Monte Carlo approach to sample the blow-up times distribution. We construct many samples of the stochastic solution, each derived with a distinct noise realization, using the Milstein approach covered in Section 3.2.2. Next we estimate the maximum existence time for every sample using the formula 2.16. This is done by performing a least-squares fit to the data τ_R vs. R using the formula:

$$\tau_R = T^\infty - \alpha R^\beta, \tag{4.2.1}$$

T^∞, $\alpha < 0$, and $\beta < 0$ parameters that need to be determined.

In Figure 4.3a the accumulated mean of the random variable T^∞ is shown for different values of the noise amplitude ρ. We observe that as the amplitude of the noise ρ increases, the mean of the blow-up time also increases. Additionally, the blow-up in the solution of the stochastic case tends to occur later compared to the blow-up time in the deterministic case.

In Figure 4.3b, the relative error with respect to the accumulated mean blow-up time is presented in function of the number of Monte Carlo realizations. As expected, the error decreases slowly due to the slow convergence rate of Monte Carlo methods $O\left(\frac{1}{\sqrt{m}}\right)$. These results also show that as ρ increases, a larger number of samples is necessary to achieve a small error.

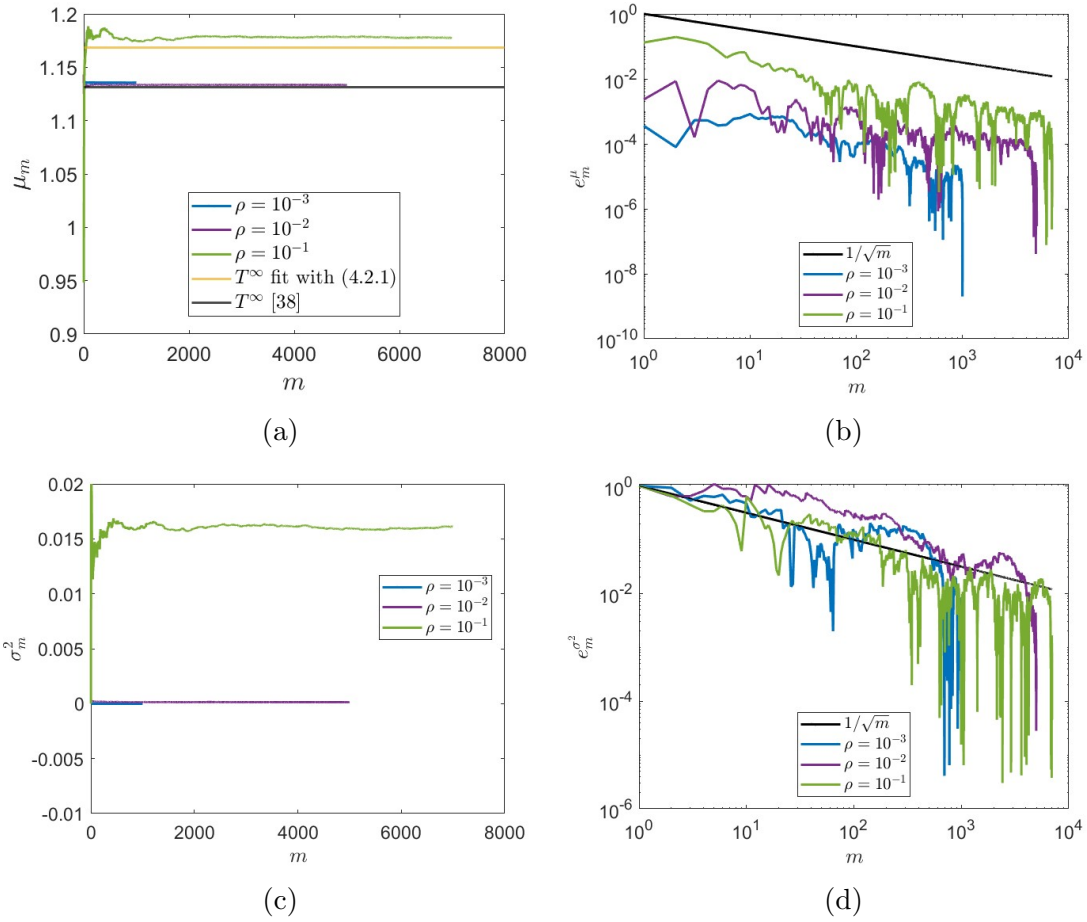

Figure 4.3: (a) Accumulated mean and (c) variance of the blow-up time estimates for various noise amplitudes. The black line in (a) represents the blow-up time estimate in the deterministic case for refined spatial resolution while the yellow line in (a) is the deterministic blow-up time estimated by algebraic extrapolation fit (4.2.1). (b) and (d) Relative errors of the accumulated mean and variance of the blow-up time estimates for different noise amplitudes, respectively. The black curve in (b) and (d) illustrates the function $\frac{1}{\sqrt{m}}$. We used 1,000 samples for $\rho = 10^{-3}$, 5,000 samples for $\rho = 10^{-2}$, and 7,000 samples for $\rho = 10^{-1}$.

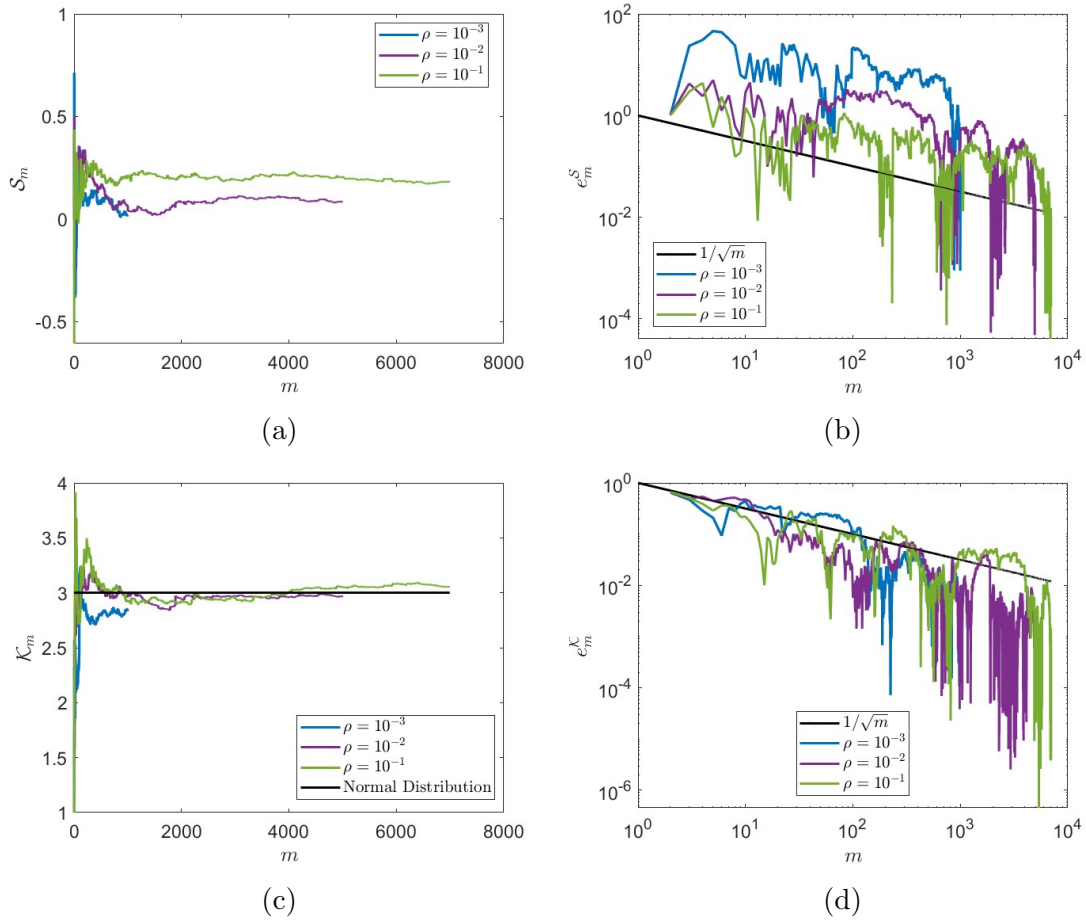

Figure 4.4: (a) Skewness and (c) Kurtosis of the blow-up time estimates for various noise amplitudes. The black line in (c) represents the normal distribution. (b) and (d) Relative errors of the skewness and kurtosis of the blow-up time estimates for different noise amplitudes, respectively. The black curve of (b) and (d) illustrates the function $\frac{1}{\sqrt{m}}$. We used 1,000 samples for $\rho = 10^{-3}$, 5,000 samples for $\rho = 10^{-2}$,and 7,000 samples for $\rho = 10^{-1}$.

In Figures 4.3c and 4.3d, the accumulated variance of the blow-up time estimates and the corresponding relative errors are depicted. We note that with increasing ρ, the variance increases, indicating a greater variability in blow-up times. The relative errors decrease slowly, similar to the mean, necessitating more samples for higher ρ.

Figures 4.4a and 4.4b show the skewness of the blow-up time estimates and the corresponding relative errors. The skewness reveals an asymmetry in the distribution of blow-up times, and as ρ increases, the distribution becomes more skewed. The relative errors in skewness also follow the $O\left(\frac{1}{\sqrt{m}}\right)$ trend.

Lastly, Figures 4.4c and 4.4d present the kurtosis of the blow-up time estimates and the corresponding relative errors. The kurtosis quantifies the presence of rare events usually associated with algebraic, rather than exponential, tails of the PDFs. Higher ρ values result in higher kurtosis, suggesting more outliers. The relative errors in kurtosis similarly decrease slowly with the number of samples, adhering to the expected Monte Carlo convergence rate.

Figure 4.5 presents the probability density functions (PDFs) of the blow-up times for various noise amplitudes ρ. As ρ grows, these histograms are increasingly skewed towards longer blow-up times, indicating longer blow-up times in comparison to the deterministic case. When compared with the deterministic blow-up time, as determined in [38], the mean blow-up time for $\rho = 0.1$ is notably higher. Conversely, for $\rho = 0.001$, the mean of the PDF closely aligns with the value in the deterministic case. The distribution for $\rho = 0.01$ is intermediate between these two extremes. Hence, for small noise magnitudes the PDFs of the maximum existence time have distributions close to the Gaussian distribution whereas, for increasing ρ they develop "heavy" tails and become skewed towards longer times. Interestingly, this increasing

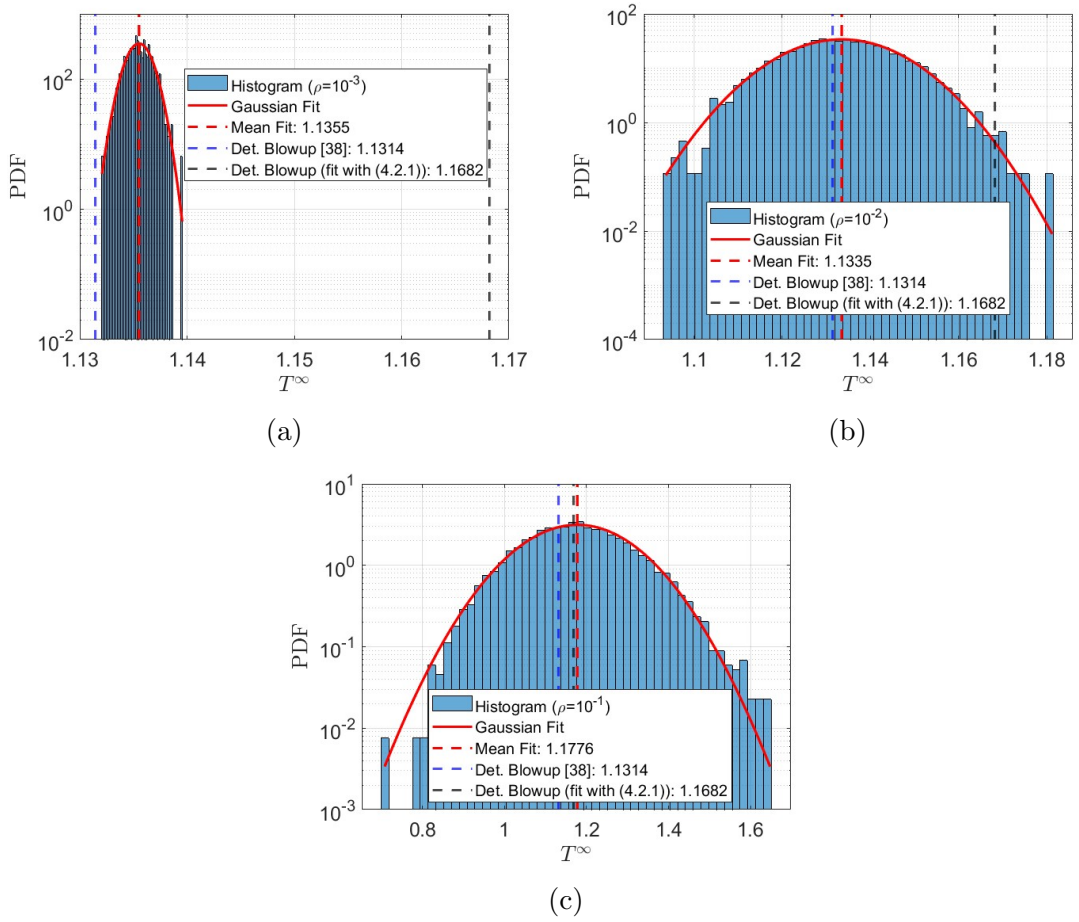

Figure 4.5: Histograms depicting the distributions of blow-up times for solutions of the stochastic problem (2.7) with varying noise amplitudes: (a) $\rho = 10^{-3}$, (b) $\rho = 10^{-2}$, and (c) $\rho = 10^{-1}$. The red curves represent the corresponding normal distribution. The red vertical lines indicate the mean of the Normal curve for each case, while the black lines denote the blow-up time in the deterministic case with extrapolation (4.2.1) and the blue line depicts the blow-up time in the deterministic case with a finer spatial resolution [38].

non-Gaussianity of the distributions is accompanied by a shift of the mean value of T^{∞} towards longer times. Therefore, realizations with longer maximum existence times become more likely. This suggests that increasing the noise amplitude ρ has a regularizing effect on the blow-up of the solution of the fractional Burgers equation in the supercritical regime, as predicted by the Theorem 2.2.2.

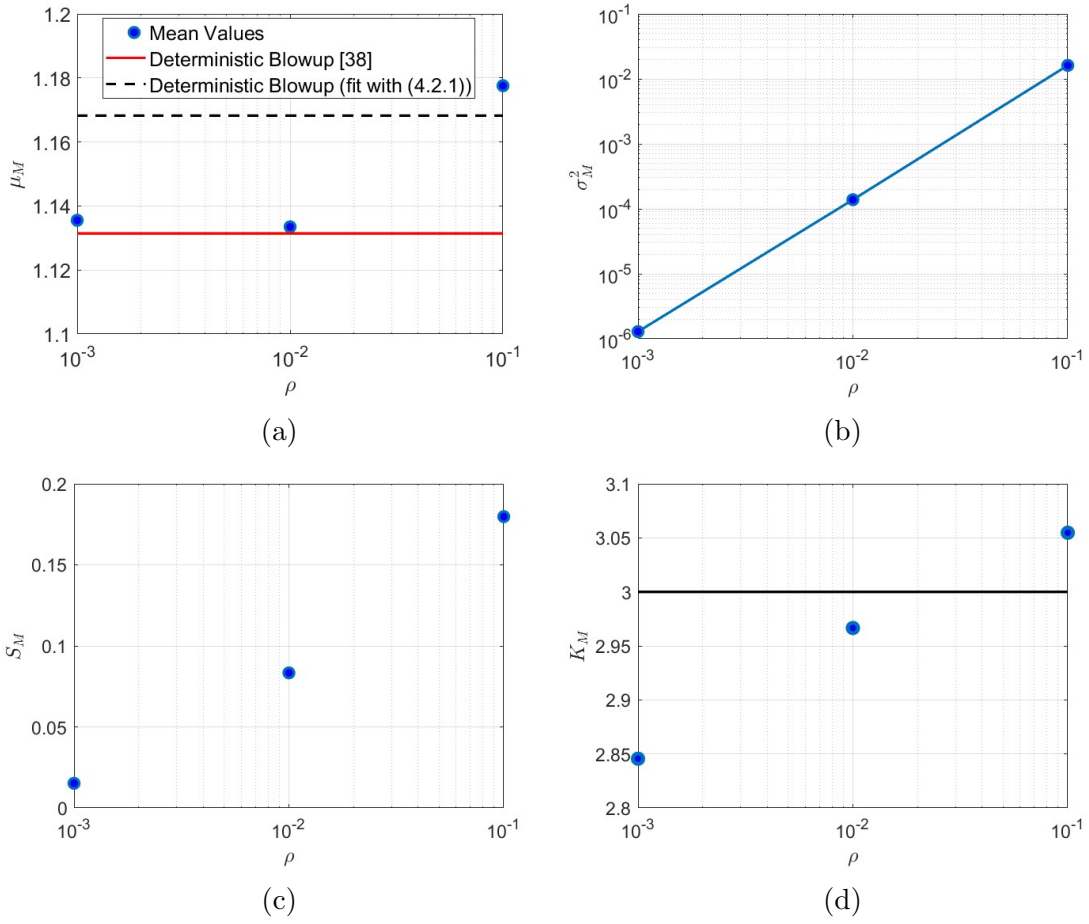

Figure 4.6: (a) Mean and (b) variance of the blow-up time T^{∞} as functions of ρ. The black line in (a) represents the blow-up time obtained with the deterministic case for algebraic extarpolation fit (4.2.1) and the red line in (a) potray the blow up time for deterministic case with finer spatial resolution [38]. (c) Skewness as a function of the noise amplitude ρ. (d) Kurtosis as a function of the noise amplitude ρ. The black line in (d) represents for the kurtosis of normal distribution.

Ultimately, Figure 4.6 displays the estimated mean T^{∞} together with its variation, skewness, and kurtosis as functions of ρ. As is evident from Figure 4.6a, the mean T^{∞} increses with ρ and for $\rho = 0.1$ becomes greater than the blow-up time T^{∞} in the deterministic case. Subsequently, Figure 4.6b shows that the variation of the T^{∞} increases with ρ, following a power-law trend. Since the slope of the line in the log-log plot is 3, the power law exponent is 3. Figures 4.6c and 4.6d demonstrate how skewness and kurtosis increase with increasing ρ, indicating that the distribution becomes more non-Gaussian.

Figure 4.7 displays the evolution of enstrophy in stochastic realizations with the highest and lowest values of T^{∞} for noise amplitudes $\rho = 10^{-3}$, $\rho = 10^{-2}$, and $\rho = 10^{-1}$, compared to the deterministic case. For $\rho = 10^{-3}$, the stochastic enstrophy aligns closely with the deterministic case, indicating minimal impact from the noise. At $\rho = 10^{-2}$, there is a significant divergence, accompanied by a noticeable delay in blow-up time. This divergence becomes even more pronounced at $\rho = 10^{-1}$, showing a broad range of behaviors and substantial delays in blow-up time. These findings emphasize that increasing the noise amplitude delays blow-up time, highlighting the significant impact of stochasticity on the fractional Burgers equation in the supercritical regime.

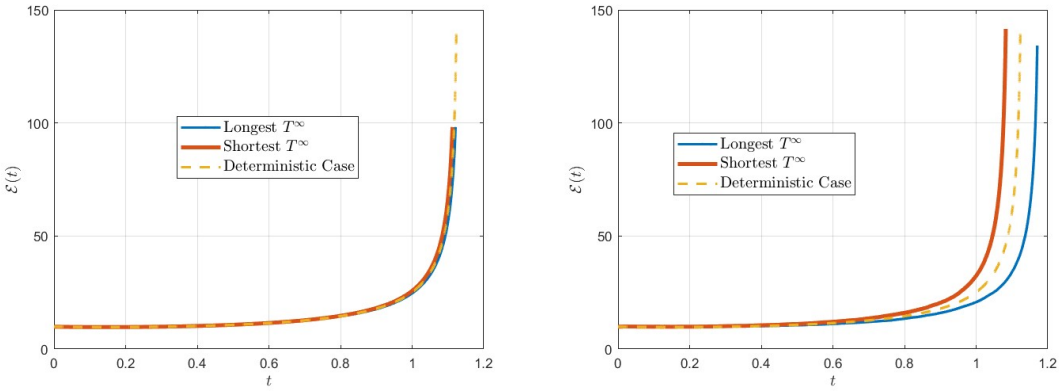

(a) (b)

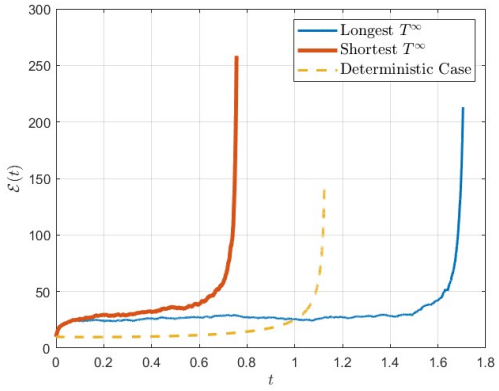

(c)

Figure 4.7: The time evolutions of the enstrophy in the stochastic realizations characterized by the longest and shortest values of maximum existence time T^∞ for (a) $\rho = 10^{-3}$, (b) $\rho = 10^{-2}$, and (c) $\rho = 10^{-1}$ deterministic case.

Chapter 5

Conclusions

The investigation focused on how stochastic excitations impact the creation of singularities and other extreme behaviors in non-linear dissipative partial differential equations, specifically the 1D fractional Burgers equation (2.4) with multiplicative colored noise. To address this question, firstly, we implemented the necessary code, combining spectrally accurate spatial discretizations with a Monte-Carlo method to ensure convergence. This allowed us to perform a series of accurate numerical calculations. Next, we devised a numerical scheme to capture the system's behavior under different noise amplitudes. This scheme enabled us to investigate the effects of multiplicative noise on the global existence of solutions. Finally, we ran extensive computations, varying the noise amplitude ρ to observe changes in the distribution of the maximum existence times T^{∞}. These experiments provided valuable data that informed our conclusions.

The investigation is driven by the question how stochastic excitations impact the creation of singularities and other extreme behaviors in non-linear dissipative partial differential equations (2.1). The 1D fractional Burgers Eq. (2.1) with multiplicative

colored noise has been considered as a model problem. By combining spectrally accurate spatial discretizations with a Monte-Carlo method in which the convergence of all approximations was meticulously verified, a series of accurate numerical calculations was performed to provide insights about the question we are interested in, as described in Theorem 2.2.2 we are interested in. This system is intriguing because it raises the question whether the magnitude of the noise, ρ, affects the global existence of solutions in the stochastic setting.

Our key conclusion is that there is some evidence that noise regularizes the emergence of singularities in the supercritical regime; that is, as the noise amplitude ρ increases, the distribution of the maximum existence times T^∞ (interpreted as a stochastic variable) becomes more non-Gaussian. It is interesting to note that when ρ grows, the mean maximum existence time likewise becomes larger, increasing the likelihood of solutions with noticeably longer maximum existence durations. This is due to the fact that as ρ grows, the PDFs of T^∞ get increasingly skewed and form heavier tails towards long maximum existence times. Under this method, increasing ρ beyond $1 \cdot 10^{-1}$ with the current time step leads to numerical instabilities. Decreasing the time step to maintain stability would result in prohibitively long computation times, making it impractical.

Reference [38] reports no evidence that additive noise prevents singularity formation in the supercritical regime. In contrast, our results indicate that multiplicative noise might regularize solutions by postponing blow-up. Specifically, as the noise amplitude ρ increases, the distribution of the maximum existence times T^∞ in our study suggests a delay in blow-up. Furthermore, while Reference [38] finds a non-monotonic decrease in the mean maximum existence time with increasing additive

noise, our observations show an increase in the mean maximum existence time with higher multiplicative noise amplitudes.

Our numerical observations, though limited by the computational constraints, indicate that larger noise amplitudes may help in postponing blow-up, aligning with the Theorem 2.2.2's implication that sufficient noise can lead to global existence and decay of the solution over time. However, further exploration with significantly larger noise magnitudes is needed to conclusively determine the regularizing effect and the required noise magnitude to prevent blow-up.

In conclusion, the answer to the query concerning the impact of stochastic excitations on isolated and extreme behavior in fractional Burgers flows is clear from the explanation above. Our results suggest that there is a possibility that noise regularizes solutions in the supercritical regime by postponing blow-up. It is still an open topic if these tendencies will hold for considerably larger noise amplitudes. Also, will we be able to prevent blow-up by increasing the noise amplitude and if prevention is possible, what will be the required noise magnitude?

Appendix A

Itô Integrals and Their Properties

A.1 Introduction to Itô Integrals

Itô calculus extends classical calculus to random processes such as Brownian motion (Wiener process). Itô integrals are crucial in stochastic calculus, with applications in mathematical finance, differential equations with noise, and other fields where stochastic models describe inherent uncertainties. This appendix provides a foundational understanding of Itô integrals, focusing on their definitions, properties, and examples [32].

A.2 Definitions and Basic Concepts

Definition A.2.1 (Predictable Process)**.** *A stochastic process* $\{X(t) : t \in [0,T]\}$ *is* ***predictable*** *if there exist an* F_t*-adapted and left-continuous processes* $\{X_n(t) : t \in [0,T]\}$ *such that* $X_n(t) \to X(t)$ *as* $n \to \infty$ *for all* $t \in [0,T]$*.*

Definition A.2.2 ($S_N^X(t)$)**.** *.Let* $\{t_0, t_1, \ldots, t_N\}$ *be a partition of* $[0,T]$ *such that* $0 =$

$t_0 < t_1 < \cdots < t_N = T$. *Then,*

$$S_N^X(t) = \sum_{j=0}^{N-1} X(t_j) 1_{[t_j, t_{j+1})}(t),$$

where $1_{[t_j,t_{j+1})}(t)$ *is the indicator function of the interval* $[t_j, t_{j+1})$.

Definition A.2.3 (Banach Space L_T^2)**.** *Let* L_T^2 *denote the space of predictable real-valued processes* $\{X(t) : t \in [0,T]\}$ *with*

$$\|X\|_{L_T^2} := \left(\mathbb{E}\left[\int_0^T |X(s)|^2 \, ds \right] \right)^{1/2} < \infty.$$

Then, L_2^T *is a Banach space with the norm* $\|\cdot\|_{L_2^T}$.

Definition A.2.4 (Itô Isometry)**.** *The Itô isometry is given by:*

$$\mathbb{E}\left[\left(\int_0^t X(s) \, dW(s) \right)^2 \right] = \int_0^t \mathbb{E}[|X(s)|^2] \, ds, \tag{A.2.1}$$

where the left-hand side represents the $L^2(\Omega)$ *norm squared of the Itô integral.*

Definition A.2.5 (Itô Integral)**.** *Let* $W(t)$ *be an* F_t*-Brownian motion and let* $X \in L_2^T$. *By definition,* X *equals the limit in* L_2^T *of a sequence of left-continuous and* F_t*-adapted processes* $X_n(t)$, $n \in \mathbb{N}$. *The stochastic integral* $I_n(t) = \int_0^T X_n(s) \, dW(s)$ *is well defined by Theorem A.3.1 and, from equation A.2.1 with* $X = X_n - X_m$,

$$\|I_n(T) - I_m(T)\|_{L^2(\Omega)} = \mathbb{E}\left[(I_n(T) - I_m(T))^2 \right] = \int_0^T \mathbb{E}\left[(X_n(s) - X_m(s))^2 \right] \, ds.$$

Then, $I_n(T)$ *is a Cauchy sequence in* $L^2(\Omega)$, *and the Itô integral* $\int_0^t X(s) \, dW(s)$ *is defined as* $\lim_{n\to\infty} \int_0^t X_n(s) \, dW(s)$ *in* $L^2(\Omega, \mathcal{F}_t)$.

A.3 Itô Integral Properties and Examples

Theorem A.3.1. *Let W_t be an F_t-Brownian motion and let $\{X(t) : t \in [0,T]\}$ be an F_t-adapted process with left-continuous sample paths.*

1. *$S_N^X(t) : t \in [0,T]$ is F_t-adapted and has continuous sample paths.*

2. *$\mathbb{E}[S_N^X(t)|F_{s_j}] = S_N^X(s_j)$ for $0 \le s_j \le t$ almost surely. In particular, $\mathbb{E}[S_N^X(t)] = 0$.*

3. *If $Y(t) : t \in [0,T]$ is also F_t-adapted with left-continuous sample paths and both $X, Y \in L^2(\Omega, L_2^T(0,T))$, then for $t_1, t_2 \in [0,T]$,*

$$\mathbb{E}[S_N^X(t_1) S_M^Y(t_2)] \to \int_0^{(t_1 \wedge t_2)} \mathbb{E}[X(s)Y(s)]\, ds \quad \text{as } N, M \to \infty.$$

Theorem A.3.2 (Itô Integral Process)**.** *Let $X \in L_2^T(\mathbb{R}^{d\times m})$. The following hold:*

1. *$(\int_0^t X(s)\, dW(s))_{t\in[0,T]}$ is a $\mathcal{F}_t$ predictable process.*

2. *The martingale property holds: for $0 \le r \le t \le T$,*

$$\mathbb{E}\left[\int_0^t X(s)\, dW(s) \middle| F_r\right] = \int_0^r X(s)\, dW(s), \text{ almost surely,}$$

   and the integral has mean zero: $\mathbb{E}[\int_0^t X(s)\, dW(s)] = 0$.

3. *For $X, Y \in L_2^T(\mathbb{R}^{d\times m})$,*

$$\mathbb{E}\left[\left(\int_0^{t_1} X(s)\, dW(s), \int_0^{t_2} Y(s)\, dW(s)\right)\right] = \int_0^{(t_1\wedge t_2)} \sum_{i=1}^m \mathbb{E}\left[\langle X_i(s), Y_i(s)\rangle\right] ds,$$

   where $\langle \cdot, \cdot \rangle$ is the $\mathbb{R}^d$ inner product.

Example: *Consider the stochastic integral* $I(t) = \int_0^t W(s)\, dW(s)$*, for* $t \geq 0$*. The martingale property gives* $\mathbb{E}[I(t)] = 0$*. The Itô isometry gives:*

$$\mathbb{E}\left[I(t)^2\right] = \int_0^t \mathbb{E}[W(s)^2]\, ds = \int_0^t s\, ds = \frac{1}{2}t^2,$$

and

$$\mathbb{E}[I(t)I(s)] = \int_0^{\min(s,t)} \mathbb{E}[W(r)^2]\, dr = \int_0^{\min(s,t)} r\, dr = \frac{1}{2}(\min(s,t))^2.$$

As Itô integrals have mean zero, $\mathrm{Cov}(I(s), I(t)) = \frac{1}{2}(\min(s,t))^2$.

Bibliography

[1] S. Albeverio and O. Rozanova. The non-viscous Burgers equation associated with random position in coordinate space: A threshold for blow up behaviour. *Mathematical Models and Methods in Applied Sciences*, 19(05):749–767, 2009. doi: 10.1142/S0218202509003607.

[2] S. Albeverio and O. Rozanova. Suppression of unbounded gradients in an SDE associated with the Burgers equation. *Proceedings of the American Mathematical Society*, 138(1):241–251, 2010. URL `http://www.jstor.org/stable/40590613`.

[3] D. Ayala and B. Protas. On maximum enstrophy growth in a hydrodynamic system. *Physica D*, 240:1553–1563, 2011. doi: 10.1016/j.physd.2011.05.010.

[4] J. Bec and K. Khanin. Burgers turbulence. *Phys. Rep.*, 447(1-2):1–66, 2007. doi: 10.1016/j.physrep.2007.04.002.

[5] M. Ben-Artzi. Global solutions of two-dimensional Navier-Stokes and Euler equations. *Archive for Rational Mechanics and Analysis*, 128:329–358, 1994. doi: 10.1007/BF00387712. URL `https://link.springer.com/article/10.1007/BF00387712`.

[6] T. Bewley. *Numerical Renaissance*. Renaissance Press, 2009.

[7] A. Boritchev. Decaying turbulence in the generalised Burgers equation. *Archive for Rational Mechanics and Analysis*, 214(1):331–357, 2014. doi: 10.1007/s00205-014-0766-5.

[8] A. Boritchev. Decaying turbulence for the fractional subcritical Burgers equation. *Discrete Contin. Dyn. Syst.*, 38(5):2229–2249, 2018. doi: 10.3934/dcds.2018092. URL `https://www.aimsciences.org/article/doi/10.3934/dcds.2018092`.

[9] Z. Brzeźniak and L. Debbi. On stochastic Burgers equation driven by a fractional Laplacian and space-time white noise. *Unknown Journal*, Unknown Year.

[10] T. Buckmaster and V. Vicol. Nonuniqueness of weak solutions to the Navier-Stokes equation. *Annals of Mathematics*, 189(1):101 – 144, 2019. doi: 10.4007/annals.2019.189.1.3. URL `https://doi.org/10.4007/annals.2019.189.1.3`.

[11] A. Chekhlov and V. Yakhot. Kolmogorov turbulence in a random-force-driven Burgers equation. *Physical Review E*, 51:R2739–R2742, 1995. doi: 10.1103/PhysRevE.51.R2739.

[12] A. Chekhlov and V. Yakhot. Kolmogorov turbulence in a random-force-driven Burgers equation: Anomalous scaling and probability density functions. *Physical Review E*, 52:5681–5684, 1995. doi: 10.1103/PhysRevE.52.5681. URL `http://link.aps.org/doi/10.1103/PhysRevE.52.5681`.

[13] A. Debussche and L. Menza. Numerical simulation of focusing stochastic nonlinear Schrödinger equations. *Physica D: Nonlinear Phenomena*, 162:131–154, 2002. doi: 10.1016/S0167-2789(01)00379-9. URL `https://ui.adsabs.harvard.edu/abs/2002PhyD..162..131D/abstract`.

[14] C. R. Doering. The 3d Navier-Stokes problem. *Annual Review of Fluid Mechanics*, 41:109–128, 2009. doi: 10.1146/annurev.fluid.010908.165218.

[15] X. Fan, J. Li, and J. Li. Global existence of strong and weak solutions to 2d compressible Navier–Stokes system in bounded domains with large data and vacuum. *Archive for Rational Mechanics and Analysis*, 245(1):239–278, 2022. ISSN 1432-0673. doi: 10.1007/s00205-022-01790-4.

[16] C. Fefferman. Existence and smoothness of the Navier-Stokes equation, 2000.

[17] F. Flandoli. *Random Perturbation of PDEs and Fluid Dynamic Models*. Lecture Notes in Mathematics. Springer, 2015.

[18] B. Gess et al. Random attractors for a class of stochastic partial differential equations driven by general additive noise. *Journal of Differential Equations*, 251(4-5):1225–1253, 2011. doi: 10.1016/j.jde.2011.02.013. URL `https://www.sciencedirect.com/science/article/pii/S0022039611001045`.

[19] J. D. Gibbon. Regularity and singularity in solutions of the three-dimensional Navier–Stokes equations. *Proceedings of the Royal Society A: Mathematical, Physical and Engineering Sciences*, 466:2587–2604, 2010. doi: 10.1098/rspa.2009.0642.

[20] M. B. Giles. Multilevel Monte Carlo Path simulation. *Operations Research*, 56 (3):607–617, 2008.

[21] M. Gubinelli and M. Jara. Regularization by noise and stochastic Burgers equations. *Stochastic Partial Differential Equations: Analysis and Computations*, 1: 325–350, 2013. doi: 10.1007/s40072-013-0011-5.

[22] M. Hairer. Solving the KPZ equation. *Annals of Mathematics, Second Series*, 178(2):559–664, 2013. doi: 10.4007/annals.2013.178.2.2. URL `https://www.jstor.org/stable/23470800`.

[23] D. J. Higham. An algorithmic introduction to numerical simulation of stochastic differential equations. *SIAM Review*, 43(3):525–546, 2001.

[24] A. Jentzen. Pathwise numerical approximations of SPDEs with additive noise under non-global Lipschitz coefficients. *Potential Analysis*, 31:375–404, 2009. doi: 10.1007/s11118-009-9139-3. URL `https://link.springer.com/article/10.1007/s11118-009-9139-3`.

[25] A. Jentzen and M. Roeckner. A Milstein scheme for SPDEs. *Foundations of Computational Mathematics*, 15, 01 2010. doi: 10.1007/s10208-015-9247-y.

[26] N. Katz and N. Pavlović. A cheap Caffarelli-Kohn-Nirenberginequality for the Navier–Stokes equation with hyper-dissipation. *Geom. Funct. Anal. GAFA*, 12 (2):355–379, 2002. doi: 10.1007/s00039-002-8250-z.

[27] A. Kiselev, F. Nazaraov, and R. Shterenberg. Blow up and regularity for fractal Burgers equation. *Dynam. Partial Differ. Equ.*, 5:211–240, 2008.

[28] C. Klein and J.-C. Saut. A numerical approach to blow-up issues for dispersive perturbations of Burgers' equation. *Physica D*, 295–296:46–65, 2015. doi: 10.1016/j.physd.2014.12.003. URL `https://arxiv.org/abs/1401.1390`.

[29] P. E. Kloeden and E. Platen. *Numerical Solution of Stochastic Differential Equations*. Springer-Verlag, Berlin, Heidelberg, 1992.

[30] R. Kruse. Optimal error estimates of Galerkin finite element methods for stochastic partial differential equations with multiplicative noise. *IMA Journal of Numerical Analysis*, 34(1):217–251, 2014. doi: 10.1093/imanum/drs055.

[31] J. Li, J. Li, and B. Lü. Global classical solutions to the full compressible Navier-Stokes system in 3d exterior domains.

[32] G. J. Lord, C. E. Powell, and T. Shardlow. *An introduction to Computational Stochastic PDEs*. Cambridge University Press, July 2014.

[33] G. N. Milstein. Approximate integration of stochastic differential equations. *Theory of Probability Its Applications*, 19(3):557–562, 1975. doi: 10.1137/1119062. URL `https://epubs.siam.org/doi/pdf/10.1137/1119062`.

[34] S. Montgomery-Smith. Global regularity of the Navier-Stokesequation on thin three-dimensional domains with periodic boundary conditions. *Electronic Journal of Differential Equations*, 1999(11):1–19, 1999. ISSN 1072-6691. URL `http://ejde.math.swt.eduorhttp://ejde.math.unt.edu`.

[35] T. E. Moschandreou. Incompressible Navier Stokes equations: Finite time blowup for a special class of initial conditions, Wave structure subject to special auxiliary equations. *Recent Advances in Mathematical Research and Computer Science*, 8:143–159, 2022. doi: 10.9734/bpi/ramrcs/v8/2515C.

[36] D. Poças and B. Protas. Transient growth in stochastic Burgers flows. *Discrete and Continuous Dynamical Systems Series B*, 23:2371, 2018. doi: 10.3934/dcdsb.2018052.

[37] E. Ramírez. Singularity formation in the deterministic and stochastic fractional burgers equations. Master's thesis, McMaster University, Hamilton, Ontario, Canada, 2020. URL http://hdl.handle.net/11375/25858.

[38] E. Ramírez and B. Protas. Singularity formation in the deterministic and stochastic fractional Burgers equation. *Physica D (Nonlinear Phenomena)*, 440:133432, 2022. doi: 10.1016/j.physd.2022.133432. URL https://www.sciencedirect.com/science/article/pii/S0167278922001713.

[39] J. C. Robinson. The Navier–Stokes regularity problem. *Philosophical Transactions of the Royal Society A*, 378(20190526), 2020. doi: 10.1098/rsta.2019.0526.

[40] M. Röckner and Z. Sobol. Kolmogorov equations in infinite dimensions: Well-posedness and regularity of solutions, with applications to stochastic generalized Burgers equations. *The Annals of Probability*, 34(2):663–727, 2006. doi: 10.1214/009117905000000666.

[41] M. Röckner, R. Zhu, and X. Zhu. Local existence and non-explosion of solutions for stochastic fractional partial differential equations driven by multiplicative noise. *Stochastic Processes and their Applications*, 124(5):1974–2002, 2014. doi: 10.1016/j.spa.2013.11.009. URL https://ideas.repec.org/a/eee/spapps/v124y2014i5p1974-2002.html.

[42] C. Sulem, P.-L. Sulem, and H. Frisch. Tracing complex singularities with spectral methods. *Journal of Computational Physics*, 50(1):138–161, Apr 1983. doi: 10.1016/0021-9991(83)90045-1. URL https://doi.org/10.1016/0021-9991(83)90045-1.

[43] A. Tambue and J. D. Mukam. Magnus-type integrator for non-autonomous SPDEs driven by multiplicative noise. *Discrete and Continuous Dynamical Systems*, 40(5):2977–3001, 2020. doi: 10.3934/dcds.2020194. URL `https://www.aimsciences.org/article/doi/10.3934/dcds.2020194`.

[44] L. N. Trefethen. *Spectral Methods in MATLAB*. SIAM, 2000.

[45] V. A. Vaygant and A. V. Kazhikhov. On existence of global solutions to the two-dimensional Navier-Stokes equations for a compressible viscous fluid. *Siberian Mathematical Journal*, 36(6), 1995. doi: 10.1007/BF02828017. URL `https://link.springer.com/article/10.1007/BF02828017`.

[46] X. Wang and S. Gan. A Runge-Kutta type scheme for nonlinear stochastic partial differential equations with multiplicative trace class noise. *Numerical Algorithms*, 62, 06 2011. doi: 10.1007/s11075-012-9568-8.

[47] X. Wang and S. Gan. Weak convergence analysis of the linear implicit Euler method for semilinear stochastic partial differential equations with additive noise. *Journal of Mathematical Analysis and Applications*, 398(1):151–169, 2013. doi: 10.1016/j.jmaa.2012.08.038.

[48] Y. Ye and C. Dou. Global weak solutions to 3d compressible Navier–Stokes–Poisson equations with density-dependent viscosity. *Journal of Mathematical Analysis and Applications*, 455(1):180–211, 2017. doi: 10.1016/j.jmaa.2017.05.081. URL `https://www.sciencedirect.com/science/article/pii/S0022247X17305048`.

[49] D. Yun and B. Protas. Maximum rate of growth of enstrophy in solutions of the

fractional Burgers equation. *Journal of Nonlinear Science*, 28:395–422, 2018. doi: 10.1007/s00332-017-9422-y. URL `https://arxiv.org/abs/1610.09578`.

[50] O. Zikanov, A. Thess, and R. Grauer. Statistics of turbulence in a generalized random-force-driven Burgers equation. *Physics of Fluids*, 9(5):1362–1367, 1997. doi: 10.1063/1.869250.